Chapter 3

Harmonic Analysis of the Wind Energy Conversion System Connected with Electrical Network

Emmanuel Hernández Mayoral,
Miguel Ángel Hernández López,
Hugo Jorge Cortina Marrero and
Reynaldo Iracheta Cortez

Additional information is available at the end of the chapter

http://dx.doi.org/10.5772/intechopen.74584

Abstract

A harmonic analysis for a wind energy conversion system (WECS) based in a doubly fed induction generator (DFIG) is presented. A *back-to-back* frequency converter as voltage source for excite to rotor winding is used whereas than the electrical network excites to stator winding. The analysis is based on the induction machine model and the steady-state frequency converter model. Additionally, dynamic-state and steady-state models are developed and compared validating the results of the simulations obtaining a harmonic model, in steady-state, clear, and precise of the wind energy conversion system.

Keywords: harmonic analysis, doubly fed induction generator, *back-to-back* frequency converter, electrical network, harmonic and inter-harmonics

1. Introduction

Energy demand is increasing day by day around the world and renewable energy has proven to be an excellent choice of competition against conventional energy sources, which produce environmental pollution and contribute to climate change and global warming. An effective and proven type of renewable energy is wind energy, which achieved an increase of 63 GW in Mexico, reaching 433 GW in total capacity worldwide. This energy has been used by the human civilization for millennia to navigate and pump water for agricultural activities. Nowadays, the wind energy is used to produce electricity that leads the world of technology. This energy is used to impulse, mechanically, the generators that produce electrical energy. The

device that allows this conversion is called wind turbine. There are different concepts regarding the coupling of the generator with the wind turbine being the most well-known fixed velocity and variable velocity wind turbines. The squirrel-cage induction generator was the first fixed velocity concept developed during the early years of wind turbines. This configuration is shown in **Figure 1**. The generator is directly connected to the electrical network but has the disadvantage of operating at low efficiency producing poor power quality. On the other hand, the double-fed induction generator (DFIG) is the technology that has the largest presence in the wind industry today as it has the advantage of have a higher energy efficiency compared to the squirrel-cage induction generator, a reduction in mechanical loads, a simple system of pitch control, and greater control of active and reactive power (see **Figure 2**). Due to the unpredictable nature of wind, wind energy still presents several challenges such as fluctuations in voltage generated and complications to achieve efficient couplings with the electrical network.

These problems have led to develop strategies to solve these mishaps. However, the devices used by these strategies produce certain alterations in the energy signal required by the generator to function properly. This implies variations in the energy delivered by the generator, which leads to a further challenge in the area of wind energy: **the power quality**. This concept describes how close the energy is to the appropriate standards to operate and allow the proper use of equipment that employ this energy. Variations in voltage can result in malfunction of sensitive components of system, a reduction in generator efficiency and in general, degradation of power quality, while harmonics, which are current and/or voltages signals occurring in electrical systems with multiple frequencies of the fundamental, can cause severe problems such as generator induction effects and torque oscillations reducing the life of generator. Therefore, it is very important to obtain a clear harmonic analysis of the wind energy conversion system (WECS) when they are excited by non-sinusoidal voltage sources since the wind industry currently lacks models for harmonic propagation studies; this is done using the Fourier transform tool described later in the chapter.

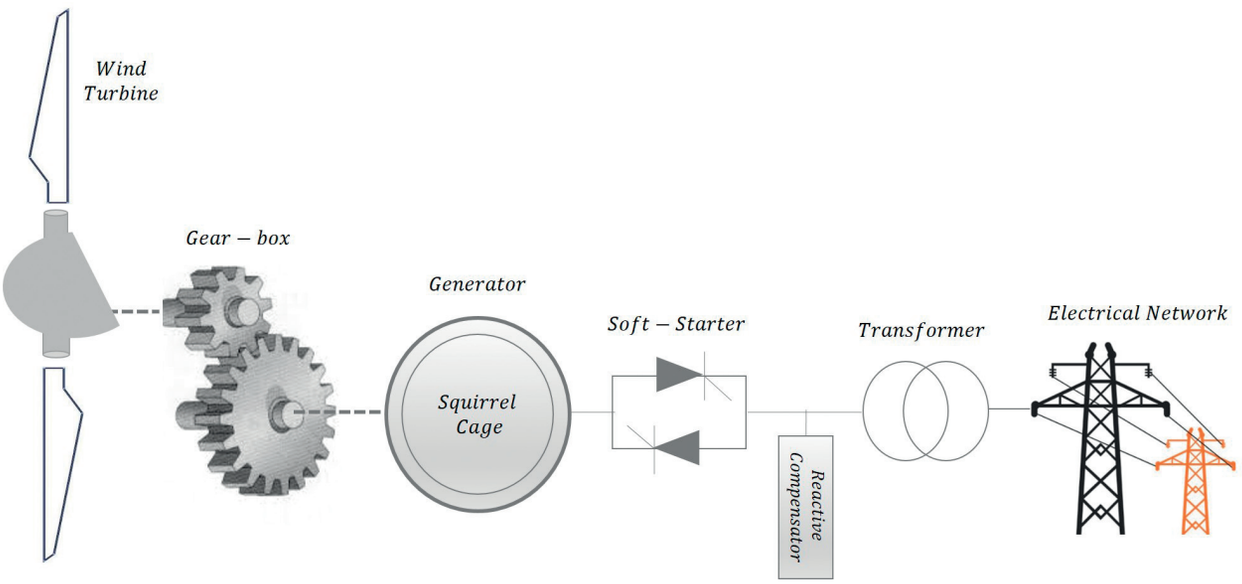

Figure 1. Configuration of squirrel-cage induction generator.

http://dx.doi.org/10.5772/intechopen.74584

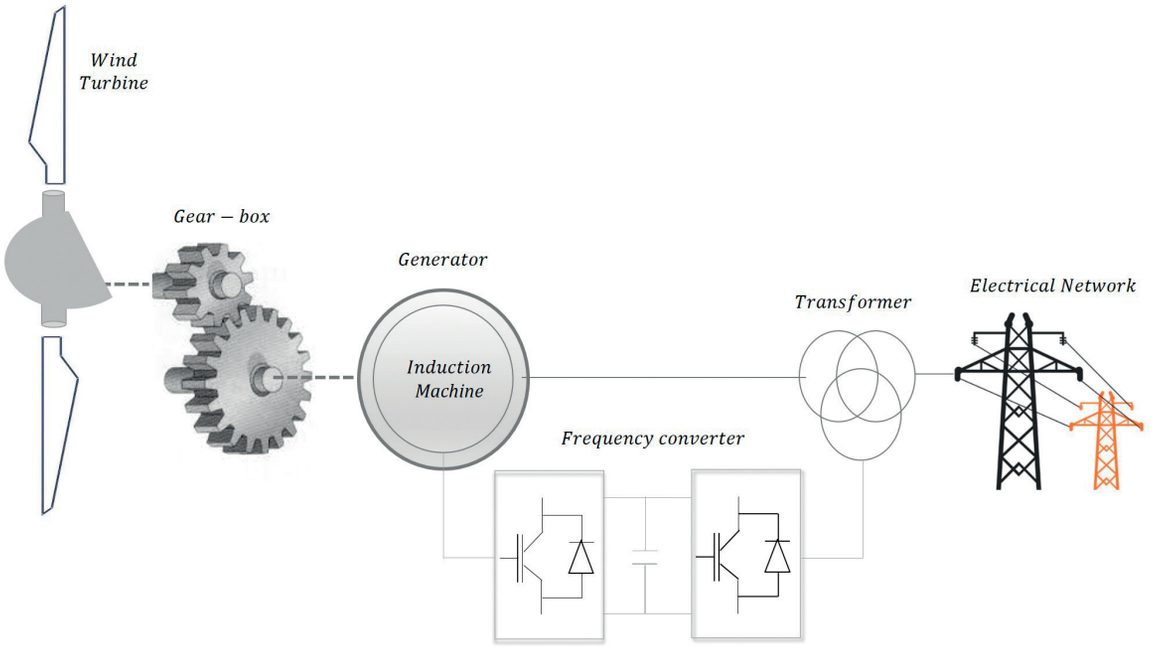

Figure 2. WECS based in doubly fed induction generator connected to the electrical network.

2. Harmonic analysis

In the beginning, Fourier series emerged as a method for the explanation of physics phenomena, at a time when there was no knowledge of electronics or telecommunications, but they are also very useful in our times applied in computer science and communication. This is possible since electrical phenomena are also physical phenomena and their behaviors explained through periodic functions or periodic wave movements, where a Fourier transform allows obtaining discontinuous waves. In addition, the harmonic analysis is the process of calculating the magnitudes and phases of the fundamental frequency and all the higher order of a periodic waveform. The resulting series is known as the Fourier series [1], which for the periodic function $\boldsymbol{X(t)}$ has the expression:

$$X(t) = a_0 + \sum_{n=1}^{\infty}\left[a_n \cos\left(\frac{2\pi nt}{T}\right) + b_n \sin\left(\frac{2\pi nt}{T}\right)\right] \quad (1)$$

This constitutes a representation in the time-domain of the periodic function. In this expression, a_0 is the average value and T is the period of the function $X(t)$, whereas a_n and b_n are the coefficients of the series for the *n-th* harmonic. These signals can be visualized in a 3-D system in which their magnitude, frequency location, and over time are represented (see **Figure 3**).

The constant term of the Fourier series is given by:

$$a_0 = \frac{1}{T}\int_{-T/2}^{T/2} X(t)dt \quad (2)$$

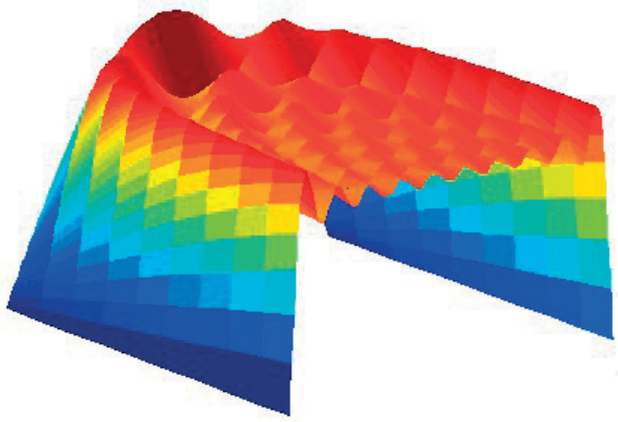

Figure 3. Harmonics signals in 3-D.

which represents the area under the curve of $X(t)$ from $-T/2$ to $+T/2$, divided by the period of the waveform T, that is the average value of the function. While a_n and b_n are given respectively by:

$$a_n = \frac{2}{T}\int_{-T/2}^{T/2} X(t)\cos\left(\frac{2\pi nt}{T}\right)dt \qquad for\ n = 1 \to \infty$$
$$b_n = \frac{2}{T}\int_{-T/2}^{T/2} X(t)\sin\left(\frac{2\pi nt}{T}\right)dt \qquad for\ n = 1 \to \infty \tag{3}$$

The above equations are simplified when the waveform has symmetry. If the waveform has odd symmetry, this is $X(t) = -X(-t)$, then a_n is zero for all values of n, and b_n is given by:

$$b_n = \frac{4}{T}\int_{0}^{T/2} X(t)\sin\left(\frac{2\pi nt}{T}\right)dt \tag{4}$$

The Fourier series for an odd function will have only sine terms. If the waveform has even symmetry, this is $X(t) = X(-t)$, then b_n is zero for all values of n, and a_n is given by:

$$a_n = \frac{4}{T}\int_{0}^{T/2} X(t)\cos\left(\frac{2\pi nt}{T}\right)dt \tag{5}$$

2.1. Transform Fourier

Formerly the process to find the Fourier transform was a bit expensive, due to the calculations that had to be done manually, nowadays with the help of technology and computers, different algorithms have been developed to simplify and make this process easier, besides of the discrete Fourier transform (DFT) and the fast Fourier transform (FFT). The main idea of the Fourier transform is to transform a signal from the time domain or space to the frequency-domain. In addition, through inverse Fourier transform, you can pass functions from the frequency-domain to the time-domain. The Fourier series therefore represents the special case of the Fourier transform applied to a periodic signal. In practice, the data are

http://dx.doi.org/10.5772/intechopen.74584

frequently available in the form of a time-sampled function, represented by a time series of amplitudes separated by fixed time intervals of limited duration. When Fourier analysis is applied to a periodic continuous signal in the time-domain produces a series of discrete frequency components in the frequency-domain [2]. The following equations form the pair of the Fourier transform:

$$\begin{aligned} X(f) &= \int_{-\infty}^{\infty} x(t)e^{-j2\pi ft}dt \\ x(f) &= \int_{-\infty}^{\infty} X(t)e^{j2\pi ft}dt \end{aligned} \tag{6}$$

where t is time, f is the frequency, $x(t)$ is the test signal, $e^{-j2\pi ft}$ is probing phasor and $X(f)$ is spectrum as a function of frequency f. Eq. (7) is called the 'forward transformation' and Eq. (8) is the 'reverse transform'. Generally, $X(f)$ is complex and can be written as:

$$X(f) = ReX(f) + jImX(f) \tag{7}$$

The real part of $X(f)$ is obtained:

$$ReX(f) = \frac{1}{2}[X(f) + X(-f)] = \int_{-\infty}^{\infty} x(t)\cos 2\pi ft\, dt \tag{8}$$

In analogous form, the imaginary part of $X(f)$ is obtained from:

$$ImX(f) = \frac{1}{2}j[X(f) - X(-f)] = \int_{-\infty}^{\infty} x(t)\sin 2\pi ft\, dt \tag{9}$$

The amplitude spectrum of the frequency signal is obtained from:

$$[x(t)] = [(ReX(f))^2 + (ImX(f))^2]^{1/2} \tag{10}$$

In addition, the phase spectrum is:

$$\emptyset(f) = tan^{-1}\left[\frac{Im\, X(f)}{Re\, X(f)}\right] \tag{11}$$

2.2. Fourier discrete transform

When frequency-domain spectrum is a sampled function, as well as the time-domain function, a Fourier transform pair of discrete components is obtained [3]:

$$\begin{aligned} X(f) &= \frac{1}{n}\sum_{n=0}^{N-1} x(t)e^{-j2\pi kn/N} \\ x(t) &= \sum_{n=0}^{n-1} X(f)e^{-j\pi kn/N} \end{aligned} \tag{12}$$

Equation (14) can be written in condensed form as:

$$[X(f)] = \frac{1}{n}[W^{kn}][x(t)] \tag{13}$$

In Eq. (15), $[X(f_k)]$ is a vector representing the N components of the function in the frequency-domain, while $[x(t)]$ is a vector representing the N samples of the function in the time-domain. The calculation of the N frequency components of N time samples requires a total of N^2 complex multiplications to solve Eq. (16).

2.3. Fourier fast transform

The implementation of Eq. (14) involves a number of complex additions and multiplications that is proportional to N^2. The term $-j2\pi kn/N$ can be calculated at one time and summarized in a table for subsequent applications; for this reason, the multiplication of k by n in this term is not normally counted as part of the implementation. The fast Fourier transform is an algorithm that allows calculating the discrete Fourier transform of a harmonic signal with a substantial saving of calculations. For the case, a number of samples equal to 2^k, where k is integer, only $(N/2)log_2(N)$ multiplications [4] are required. The saving in calculations increases as the number of samples increases with the ratio:

$$\frac{N^2}{(N/2)log_2(N)} = \frac{\ln(4)N}{\ln(N)} \tag{14}$$

Thus for 2^{10} samples, the work is reduced to analyzing only 10^3 samples, which reduces the number of operations 205 times. The algorithm that is proposed is based on the method called 'successive folding'. Knowing that $N = 2M$ where M is a positive number, so

$$F(k) = \frac{1}{2M}\sum_{n=0}^{2M-1} f(x)W_{2M}^{nk} = \frac{1}{2}\left\{\frac{1}{M}\sum_{n=0}^{M-1} f(x)\,W_{2M}^{(2x)} + \frac{1}{M}\sum_{n=0}^{M-1} f(2x+1)W_{2M}^{(2x+1)}\right\} \tag{15}$$

which can be expressed as

$$F(k) = \frac{1}{2}\left\{\frac{1}{M}\sum_{x=0}^{M-1} f(2x)W_M^{kn} + \frac{1}{M}\sum_{x=0}^{M-1} f(2x+1)W_M^{nk}W_{2M}^{k}\right\} \tag{16}$$

If it is defined as

$$F_{even}(k) = \frac{1}{M}\sum_{x=0}^{M-1} f(2x)\,W_M^{nk} \tag{17}$$

For $k = 0,1,\ldots,M-1$ and

$$F_{odd}(k) = \frac{1}{M}\sum_{x=0}^{M-1} f(2x+1)\,W_M^{nk} \tag{18}$$

For $k = 0,1,\ldots,M-1$, then we have

$$F_{(k)} = \frac{1}{2}\{F_{even}(k) + F_{odd}(k)W_{2M}^{k}\} \tag{19}$$

Also, given that $W_M^{k+M} = W_M^k$ and $W_{2M}^{k+M} = -W_{2M}^k$,

$$F(k+M) = \frac{1}{2}\{F_{even}(k) - F_{odd}(k)W_{2M}^k\} \tag{20}$$

A careful analysis of the last equations shows some interesting properties of these expressions. Note that an N-point transform can be calculated by dividing the original expression into two parts, as indicated in the last two equations. The calculation of the first half of $F(k)$ requires the evaluation of the two transforms of N/2 points according to the last equations. The resulting values of $F_{odd}(k)$ and $F_{even}(k)$ are replaced in $F_{(k)}$ for $k = 0,1,2,\ldots,(N/2-1)$. The other half is obtained by equation $F(k+M)$ without requiring additional evaluations of the transform. Considering a number of samples equal to 2^n, with n positive integer, it can be shown that the number of complex operations (multiplications and additions) is given by:

$$m(n) = 2m(n-1) + 2^{n-1} \quad n \geq 1$$

$$a(n) = 2a(n-1) + 2^n \quad n \geq 1$$

These expressions indicate the number of multiplications $(m(n))$ and sums $(a(n))$ for which $m(0)$ and $a(0)$ are equal to zero, since the transformation of a point does not require any operation. It is possible to conclude, by induction, that the number of operations, sums and complex multiplications, which is required to implement an algorithm for FFT, is given by:

$$m(n) = \frac{1}{2}2^n log_2 2^n = \frac{1}{2}Nlog_2 N = \frac{1}{2}Nn \qquad n \geq 1$$

And

$$a(n) = 2^n log_2\, 2^n = Nlog_2\, N = Nn \qquad n \geq 1$$

The application of this mathematical tool are varied, for electrical engineering, electronics, telecommunications and other fields of information sciences. All these sciences can to demonstrate that the sinusoidal signals can represent the sending of data by electrical transmission networks. In the following sections, a model of the doubly fed induction generator for harmonic analysis based on the Fourier transform is presented. Initially, the mathematical model of DFIG is presented at the fundamental frequency. Then, the model is performed at harmonic frequencies to obtain the harmonics components generated in the electrical variables of the generator. Finally, the results are compared and summarized in tables.

3. Wind turbines technologies

The connection of wind farms to an existing transmission or distribution network can affect the behavior of the same depending on two main variables:

1. Installed wind power.
2. 'Strength' to network to which its connects (expressed as PCC/P_{wind}).

This analysis must be done both from the point of view of static and dynamic behavior of the system. Unlike other types of generation technologies, it is not usual for wind generation to cause problems in terms of the harmonic, inter-harmonic and sub-harmonic distortion. This is due both to the fact that most of the machines used are of the asynchronous type, that is, the technology type of wind energy conversion system used in wind farms determines the harmonic distortion intensity. For example, the fixed velocity wind turbines based in squirrel-cage induction generator, the element that causes current distortion is the soft-starter, formed by a thyristor bridge, which not in all operations of the turbine is in operation. On the other hand, variable-velocity wind turbines today have in common the use of power electronic converters to be able to vary the velocity and to maintain the power factor within the desired limits. However, these devices produce harmonic signals in the generator and the harmonic distortion magnitude depends mainly on the type of inverter or converter and its control because these use the IGBT thyristors (isolated gates bipolar transistors). The switching frequency in these inverters is limited to the range of 2–3 kHz. The frequency converters affect waveform quality and can negatively affect other consumers connected to the electrical network.

3.1. WECS using DFIG with conventional *back-to-back* frequency converter

Considering the different types of WECS configuration, a wind turbine based on a doubly fed induction generator (DFIG) connected directly to the electrical network via a frequency converter is analysed. Among electronic power converters there are three types widely used in the wind power market: *back-to-back* converter, multilevel converter and the matrix converter [5]. In this section, the revision is made around the network-connected WECS-based DFIG and a *back-to-back* converter attached at a point common coupling (PCC). A rotor-side converter (RSC), a network-side converter (NSC) and a decoupling capacitor between the two converters constitute this converter. Notice that the harmonic distortion is a phenomenon that causes problems for both the users and the entity responsible for the provision of the electric power service [6], so it is considered necessary an appropriate understanding of the techniques currently used to mitigate this phenomenon. In this sense, the literatures that define the harmonic sources in WECS are classified as follow: Harmonic distortion from the network and harmonic distortion form the WECS:

1. The harmonic distortion from the electrical network: Since the WECS is connected to the electrical network; it becomes sensitive to any harmonic distortion coming from it. Distorted voltages in the stator generate harmonic currents in the WECS, which in turn can generate ripples voltage, torque pulsations, overheating, and increased losses in stator windings, under power factor, among others [7]. In some cases, these affections can have destructive effects on the WECS [8]. The solutions found in the literature involve the use of custom power devices as well as various control strategies implemented in the frequency converters.

2. The harmonic distortion from the WECS: The harmonics coming from the WECS is another of the harmonic distortion scenario, which the injection of harmonic components of voltage or current into the electrical network can cause problems such as excessive heating of transformers and conductors [9]. The main causes of harmonics from the WECS are: harmonics produced by nonlinear loads inherent to the generation system and harmonics produced by the WECS itself that is to say, associated to the operation of the components (generator, electronic power converter).

3.1.1. Operating principle of doubly fed induction generator

As in traditional three-phase induction generator, the doubly fed induction generators have a magnetic field formed by the stator phases rotating at synchronous velocity (ω_{es}), which is determined by the network frequency and the number of poles of the generator [10, 11], which is determined as $\omega_{es} = 2\pi f_{es}$ or $n_s = 120 \times f_{es}/p$ where f_{es} is the voltage frequency of network in Hertz, p is the poles number of generator, ω_{es} is the synchronous velocity in rad/s and n_s is the synchronous velocity in rev/min. Unlike the first generators, the frequency of the rotor currents in the doubly fed induction generator can be controlled, thanks to the operation of the converter located on the generator-side. The control of the rotational currents governs the velocity and torque characteristic curve, which allows optimizing and regulating the power generated by the DFIG [12]. In the same way that the velocity stator fields are obtained, the velocity of the rotor fields formed by the rotor currents is defined by $\omega_{er} = 2\pi f_r$ where f_r is the frequency of rotor voltage in Hertz, and ω_r is the angular velocity of rotor fields in rad/s. Then, slip s is defined as the relative velocity of the stator fields with respect to the rotor velocity ω_r, measured in per unit:

$$s = \frac{\omega_{es} - \omega_r}{\omega_{es}} \tag{21}$$

The concept 'slip' is very important because it describes the machine operation. Now, with the above equation, we can establish in $f_{er} = sf_{es}$ where f_{es} is the frequency of stator current. From this, it is possible to characterize the modes of operation of the machine, which in general in wind systems present velocity variations around 30% [13]. In order to produce a non-zero torque necessary for generator operation, the magnetic fields caused by the stator and rotor currents must rotate at the same velocity with respect to a point coupling common [14], $\omega_{es} = \omega_r + \omega_{er}$. Now, the mechanical velocity of the rotor is obtained and can be controlled according to previous equations by controlling the frequency of the rotor currents affected by the rotor-side converter. When the slip is positive, it has ω_{es} to be greater ω_r and therefore ω_{er} to be positive and the rotating magnetic fields generated by the stator and rotor coils rotate in the same direction. In this case:

$$\omega_m = \frac{2\pi(f_{es} - f_{er})}{(p/2)} \tag{22}$$

where ω_m is the rotation velocity of rotor measure with respect to stator in radians geometrics. When the slip is negative, it has ω_{es} to be minor to ω_r and therefore ω_{er} to be positive and the rotating magnetic fields generated by the stator and rotor coils rotate in the opposite direction. This means that the rotor is fed with the inverse stator sequence. Under these conditions:

$$\omega_m = \frac{2\pi(f_{es} + f_{er})}{(p/2)} \tag{23}$$

As can be seen in the equations just described, the velocity at which the rotor rotates depends exclusively on the network and rotor frequencies, and not on the torque imposed by the turbine, as is the case with other types of generators.

3.1.2. Steady-state model of DFIG at harmonic frequencies

The general scheme of doubly fed induction generator (DFIG) in the stationary reference-frame uses a wound rotor with slip rings to transmit current between the stator and rotor voltage sources is shown in **Figure 4**. The voltage equation that describes the equivalent circuit is given by

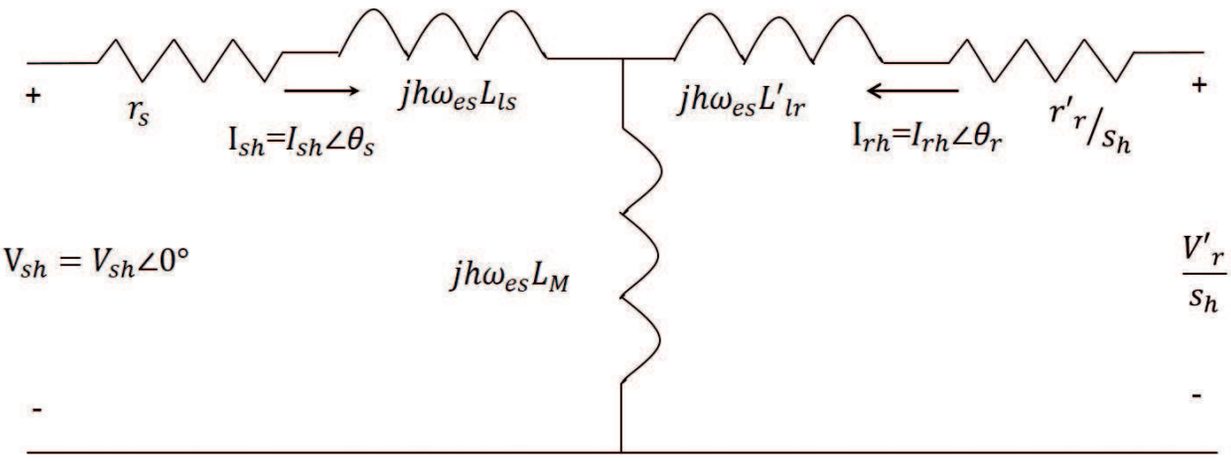

Figure 4. Steady-state equivalent circuit of the induction machine.

$$V_{sh}\angle 0° = -r_s I_{sh} - jh\omega_{es}L_{ls}I_{sh} - jh\omega_{es}L_M I_{sh} - jh\omega_{es}L_M I_{rh}$$
$$\frac{V_r}{s_h} = \frac{r_r}{s_h} I_{rh} - jh\omega_{es}L_{lr}I_{rh} - jh\omega_{es}L_M I_{rh} - jh\omega_{es}L_M I_{sh} \quad (24)$$

where V_{sh} and V'_{rh} are stator and rotor harmonic voltages, I_{sh} and I'_{rh} are the stator and rotor harmonic currents, respectively, and L_M is the magnetizing inductance given by $L_M\ 3/2\ L_{ms}$, and s_h is the harmonic slip. To calculate the slip, s_h, corresponding to the harmonic h, it is necessary to determine if the harmonic is a positive, negative or zero sequence. All multiples of three in a three-phase system are zero sequence, that is, corresponding to the harmonics $h = 3k$, and since they do not produce a rotating magnetic field, they do not contribute to the production of electric torque. The rest of the odd harmonics produce positive or negative electric torques depending on the sequence of the harmonic system generated by the rotating magnetic field, that is, the harmonics with behavior $h = 3k + 1$ and $h = 3k - 1$. Thus, the harmonic slip is defined by [15]:

$$s_h = \frac{\pm h\omega_{es} - \omega_r}{\pm h\omega_{es}} \quad (25)$$

The sign (+) and (−) is used for positive and negative sequence, respectively. In order for a harmonic of order h in a three-phase system to be in sequence positive, the following relation must be fulfilled:

$$\frac{2\pi}{3}h = \frac{2\pi}{3} + 2\pi h \ \rightarrow h = (2n-1) = 1 + 3h \ \rightarrow n = 1 + \frac{3h}{2} \quad (26)$$

Since h must be an odd number, n must belong to natural numbers; this implies that k must be a multiple of 2

$$k = 2m; \quad \forall m \in N \ \rightarrow n = 1 + 3m \ \rightarrow h = 6m + 1; \quad \forall m \in N \quad (27)$$

In order for a harmonic of order h in a three-phase system to be in sequence negative, the following relation must be fulfilled

http://dx.doi.org/10.5772/intechopen.74584

$$\frac{2\pi}{3}h = \frac{4\pi}{3} + 2\pi h \ \rightarrow h = (2n-1) = 2 + 3h \ \rightarrow n = 1 + \frac{3(h+1)}{2} \tag{28}$$

Since h must be an odd number, n must belong to natural numbers; this implies that k+1 must be a multiple of 2,

$$k + 1 = 2m; \qquad \forall\, m \in N \rightarrow n = 3m \rightarrow \mathrm{h} = 6m - 1; \qquad \forall\, m \in N, \qquad m \neq 0$$

In summary:

a. Harmonics of positive sequence: $h = 6m + 1, \ \ m = 0,1,2, \ldots$

b. Harmonics of negative sequence: $h = 6m - 1, \ \ m = 0,1,2, \ldots$

The stator and rotor phasors currents are obtained from the above equation:

$$\mathrm{I}_{sh} = \frac{-\mathrm{V}_{sh}(r_r + r_r + jhs_h\omega_{es}L_{lr}) + \mathrm{V}_{rh}(jh\omega_{es}L_M)}{(r_s r_r - s_h\omega_{es}L_{ls}\omega_{es}L_{lr} + s_h\omega_{es}L_M) + jh(r_r\omega_{es}L_{ls} + s_h r_s\omega_{es}L_{lr})}$$

$$\mathrm{I}_{rh} = \frac{\mathrm{V}_{sh}(js_h\omega_{es}L_M) - \mathrm{V}_{rh}(r_s + jh\omega_{es}L_{ls})}{(r_s r_r - s_h\omega_{es}L_{ls}\omega_{es}L_{lr} + s_h\omega_{es}L_M) + jh(r_r\omega_{es}L_{ls} + s_h r_s\omega_{es}L_{lr})} \tag{29}$$

Then, $V_{sh} = V_{sh}\angle 0°$ and $V_{rh} = V_{rh}\angle\varphi$; can be written as:

$$\begin{aligned}
\mathrm{I}_{sh} &= \frac{1}{A^2 + B^2}[-(Br_r + As_h\omega_{es}L_{lr})V_{sh} + A\omega_{es}L_M V_{rh}\cos\varphi - B\omega_{es}L_M V_{rh}\sin\varphi] \\
&+ jh\frac{1}{A^2 + B^2}[(Ar_r - Bs_h\omega_{es}L_M)V_{sh} + B\omega_{es}L_M V_{rh}\cos\varphi + A\,\omega_{es}L_M V_{rh}\sin\varphi] \\
\mathrm{I}_{rh} &= \frac{1}{A^2 + B^2}[As_h\omega_{es}L_M V_{sh} - (Br_s + A\omega_{es}L_{ls})V_{rh}\cos\varphi - (Ar_s - B\omega_{es}L_{ls})V_{rh}\sin\varphi] \\
&jh\frac{1}{A^2 + B^2}[Bs_h\omega_{es}L_M V_{sh} - (Ar_s + B\omega_{es}L_{ls})V_{rh}\cos\varphi - (Br_s - A\omega_{es}L_{ls})V_{rh}\sin\varphi]
\end{aligned} \tag{30}$$

where $A = s_h r_s\omega_{es}L_{lr} + r_r\omega_{es}L_{ls}$ and $B = r_r r_s + s_h(\omega_{es}{L_M}^2 - \omega_{es}L_{lr}\omega_{es}L_{ls})$.

3.1.3. Analysis of back-to-back converter at harmonic frequencies

One of the most used equipment in the industry for the control of doubly fed induction generators (DFIG) is the AC-AC three-phase converter. In such equipment, the voltage generated in the DC link (V_{dc}) is provided by a three-phase rectifier, either from the network voltage, or from the power generated in the rotor. This will depend on the velocity of rotation of the generator.

The controlled rectifiers allow a bidirectional flow of power and through appropriate control and modulation; techniques generate virtually sinusoidal input currents. The power factor of this type of rectifiers can be adjusted at will. It should be mentioned that in these devices, the harmonics present in the current are the same as those present in the voltage. Therefore, the ripple that appears on the voltage, just like in the current, is rippled from high frequency due to the switching function. To determine the voltage that is obtained from the inverter, first obtain the voltage in the capacitor according to the following expression:

$$C_{dc}\frac{dv0_{dc}}{dt}=\left\{\sum_{h=n}^{\infty}\left(I_{inv\_h}+I_{rect\_h}\right)\cos[\omega_{inv}+(\theta_{rect})]-\sum_{h=n}^{\infty}\left(I_{inv\_h}+I_{rect\_h}\right)\cos[h\omega_{inv}t+(\theta_{inv})]\right\} \tag{31}$$

Solving, in steady state, with $v_{inv}(0)=V_{inv}$, where V_{inv} represents the average value voltage in the inverter, we have the following expression:

$$v_{inv}=V_{inv}+\sum_{h=n}^{\infty}\frac{I_{inv\_h}}{\omega_{inv}(h-1)}sin[\omega_{inv}t(h-1)+(\vartheta_{inv}-\theta_{inv})]-\sum_{h=n}^{\infty}\frac{I_{inv\_h}}{\omega_{inv}(h-1)}sin[\omega_{inv}t(h-1)+(\vartheta_{inv}-\theta_{inv})] \tag{32}$$

To obtain the value of the inverter current, it is necessary to know the capacitor current (I_{DC}) and according to the differential equation governing the behavior of the DC bus in the frequency converter, it is known that this capacitor current is given by:

$$C_{dc}\frac{dv_{dc}}{dt}=\frac{1}{2}\left[\left(m_{inv}^{a}I_{inv}^{a}+m_{rect}^{a}I_{rect}^{a}\right)+\left(m_{inv}^{b}I_{inv}^{b}+m_{rect}^{b}I_{rect}^{b}\right)+\left(m_{inv}^{c}I_{inv}^{c}+m_{rect}^{c}I_{rect}^{c}\right)\right] \tag{33}$$

where the switching function $m \in \{-1, 0, 1\}$ is a discrete variable of the modulation SPWM, which is defined as

$$m_1^a=2S_{11}-1,\quad m_1^b=2S_{13}-1\quad and\quad m_1^c=2S_{15}-1 \tag{34}$$

whose mathematical representation can be obtained by decomposition in Fourier series by

$$m_{inv,rect}^{a}=M_{inv,rect}^{a}\,sin\left(\omega_{inv,rect}t+\theta_{inv,rect}\right)+\sum_{h=n}^{\infty}M_{inv,rect}^{a}sin\left(h\omega_{inv,rect}t+\theta_{inv,rect}\right) \tag{35}$$

where ω represents the network frequency; $M_{inv,rect}^{a}$ and $\theta_{inv.rect}$ is the magnitude and phase angle of the fundamental component of the modulation signal, respectively, whereas $M_{inv,rect\_h}^{a}$ and $\theta_{inv,rect\_h}$ represent the magnitude and phase of the harmonic component of the modulation signal. The first term of the summation provides the fundamental component and the second determines the harmonic components. On the other hand, the representation of the line current is given by

$$I_{inv,rect}^{a}=\frac{P_{r,g\,(inv,rect)}}{3V_{inv,rect}}\,sin\left(\omega_{inv,rect}t+\theta_{inv,rect}\right) \tag{36}$$

where P represents the power in inverter and $\theta_{inv,rect}$ the angle of the power factor of $V_{inv,rect}$ which is the phase-neutral effective voltage of the electrical network. Then, the current I_{inv}^{a} a is given by

$$I_{inv}^{a}=I_{inv}^{a}\,sin\left(\omega_{inv}t+\theta_{inv}\right)+\sum_{h=n}^{\infty}M_{inv\_h}^{a}I_{inv}^{a}\,sin\left(h\omega_{inv}t+\theta_{inv}\right)sin\left(h\omega_{inv}t+\theta_{inv}\right) \tag{37}$$

By analyzing only, the harmonic components, previous expression is reduced to

$$I_{inv}^{a}=\sum_{h=n}^{\infty}M_{inv\_h}^{a}I_{inv}^{a}\,sin\left(h\omega_{inv}t+\theta_{inv}\right)sin\left(h\omega_{inv}t+\theta_{inv}\right) \tag{38}$$

In addition, for *b* and *c* phases, the independent products can be calculated by

$$I_{inv}^{b} = \sum_{h=n}^{\infty} M_{inv1_h}^{b} I_{inv}^{b} \sin\left(h\omega_{inv}t + \theta_{inv} - \frac{2\pi}{3}\right) \sin\left(h\omega_{inv}t + \theta_{inv} - \frac{2\pi}{3}\right)$$
$$I_{inv}^{c} = \sum_{h=n}^{\infty} M_{inv}^{c}{}_{h} I_{inv}^{c} \sin\left(h\omega_{inv}t + \theta_{inv} + \frac{2\pi}{3}\right) \sin\left(h\omega_{inv}t + \theta_{inv} + \frac{2\pi}{3}\right) \quad (39)$$

Using the trigonometric identity:

$$sinA\ sinB = \frac{1}{2}[cos(A-B) - cos(A+B)]$$

Finally, the sum defined by the above equations is represented by

$$I_{inv} = \frac{1}{2} I_{inv}^{a} \left\{ \sum_{h=n}^{\infty} M_{inv\_h}^{a} cos[\omega_{inv}t(h-1) + (\vartheta_{inv} + \theta_{inv})] - \sum_{h=n}^{\infty} M_{inv\_h}^{a} cos[\omega_{inv}t(h+1) + (\vartheta_{inv} + \theta_{inv})] \right\} +$$
$$\frac{1}{2} I_{inv}^{b} \left\{ \sum_{h=n}^{\infty} M_{inv\_h}^{b} cos\left[\omega_{inv}t(h-1) - \frac{2\pi}{3}(h-1) + (\vartheta_{inv} - \theta_{inv})\right] - \sum_{h=n}^{\infty} M_{inv\_h}^{b} cos\left[s_{hr}\omega_{inv}t(h+1) - \frac{2\pi}{3}(\vartheta_{inv} + \theta_{inv})\right] \right\} +$$
$$\frac{1}{2} I_{inv}^{c} \left\{ \sum_{h=n}^{\infty} M_{inv\_h}^{c} cos\left[\omega_{inv}t(h-1) + \frac{2\pi}{3}(h-1) + (\vartheta_{inv} - \theta_{inv})\right] - \sum_{h=n}^{\infty} M_{inv\_h}^{c} cos\left[s_{hr}\omega_{inv}t(h+1) + \frac{2\pi}{3}(\vartheta_{inv} + \theta_{inv})\right] \right\}$$

The same procedure is performed for the network-side converter. The DC link parameter is shown in **Table 1**. **Figures 5** and **6** show the voltage generated and harmonic frequency of the rotor side converter.

Parameters	Value
DC link capacitor	32.5 F
DC link voltage	180 V
Base voltage	176.5 V
Base current	33 A
Base power	22.5 kVA

Table 1. DC link parameters.

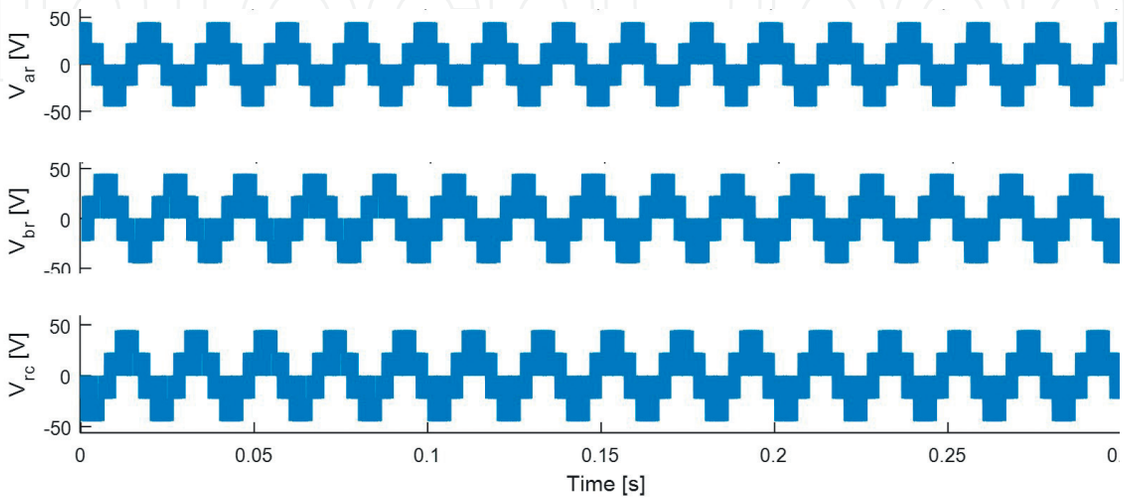

Figure 5. Voltage generated for rotor-side converter.

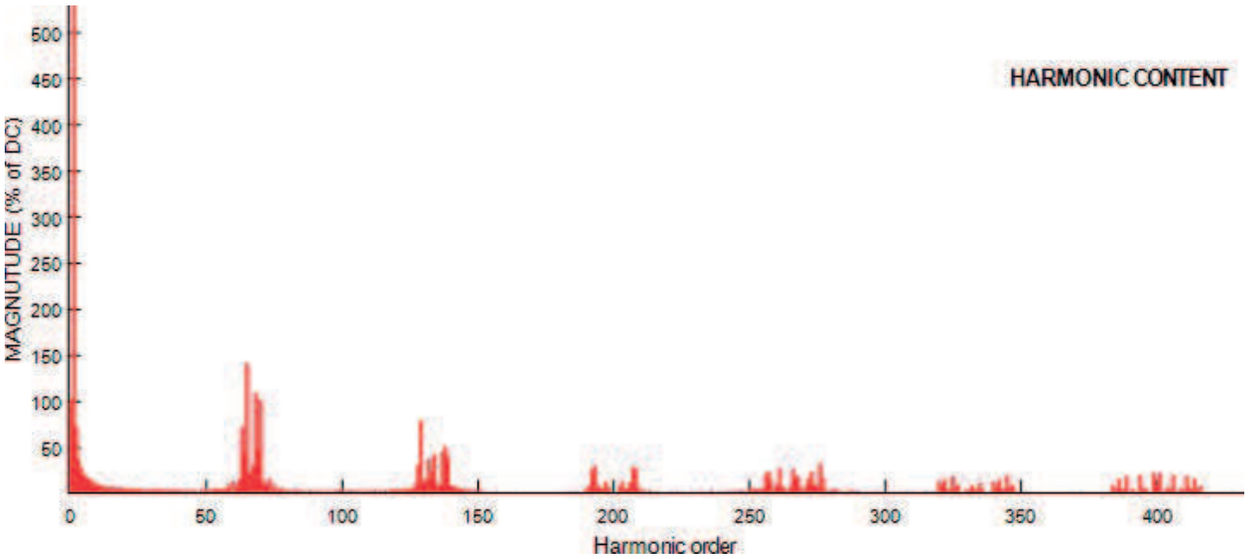

Figure 6. Harmonic frequencies of rotor-side converter.

Figures 7 and **8** show the voltage generated and the harmonic order of the network-side converter. The voltage generated by the converter and shown in **Figure 5** will be the excitation source of the rotor winding. The harmonic slip of rotor-side converter is shown in **Table 2**.

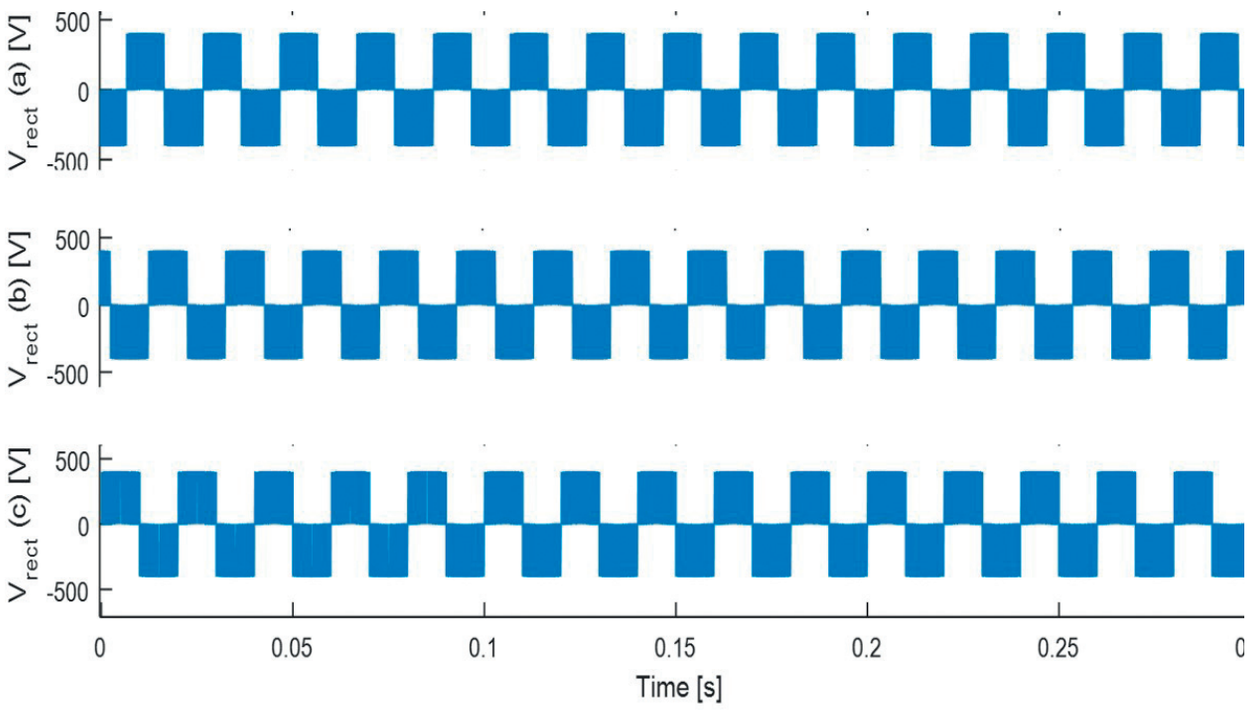

Figure 7. Voltage generated for network-side converter.

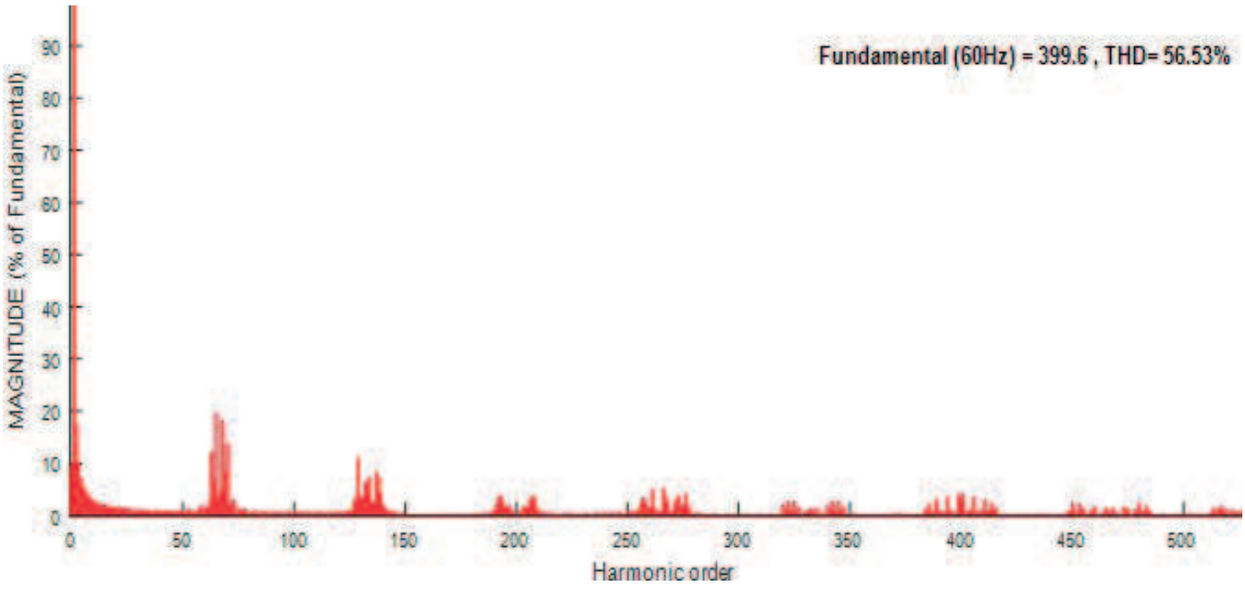

Figure 8. Harmonic order of network-side converter.

Harmonic	**5**	**7**	**11**	**13**	**17**	**76**	**80**	**158**	**159**
Sequence	—	+	—	+	—	+	—	+	—
Harmonic slip	1.21	0.96	1.32	0.97	1.25	0.98	1.01	0.993	1.07

Table 2. Harmonic slip of rotor side converter.

4. Model validation

To validate the proposed model a three-phase generator of 37.5 kW, 460 V, and 46.8 A is used. The induction generator parameters are shown in **Table 3**. Noted that the results obtained from the proposed model (steady-state) are compared with those obtained from the simulated complete model (dynamic) ones the steady-state has been reached. For this case study, a $T_m = 198\ N \cdot m$ in the induction generator was used.

4.1. Case study 1: DFIG excited with conventional *back-to-back* converter

For this case, the generator is excited in the stator windings with a sinusoidal three-phase balanced voltage source of 460 V at 60 Hz shown in **Figure 9**. Rotor windings are excited with a quasi-sine voltage source of 50 V at 45 Hz. The voltage waveforms of rotor winding are shown in **Figure 5**. The stator and rotor current waveforms obtained from dynamic-state are shown in **Figures 10** and **11**, respectively. An expansion of these currents is made once they have reached their steady-state. The electromagnetic torque and the nominal velocity reached by the generator are shown in the **Figures 12** and **13**, respectively.

Parameters	50 HP/37.5 kW
Wind speed	10 m/s
Number of poles	4
Rotor speed	1705 rpm
Inertia	1.662 kg·m^2
Nominal line current	46.8 Amps
Nominal line-to-line voltage	460 Vrms
Nominal torque	198 N.m
Nominal frequency	60 Hz
Stator resistance, r_s	0.087 Ω
Stator inductance, L_{ls}	0.0008010 H
Rotor resistance, r_r	0.228 Ω
Rotor inductance, L_{lr}	0.0008010 H
Magnetizing inductance, $L_{mr} = L_{ms}$	0.347 H

Table 3. Parameters of a 50 HP induction generator.

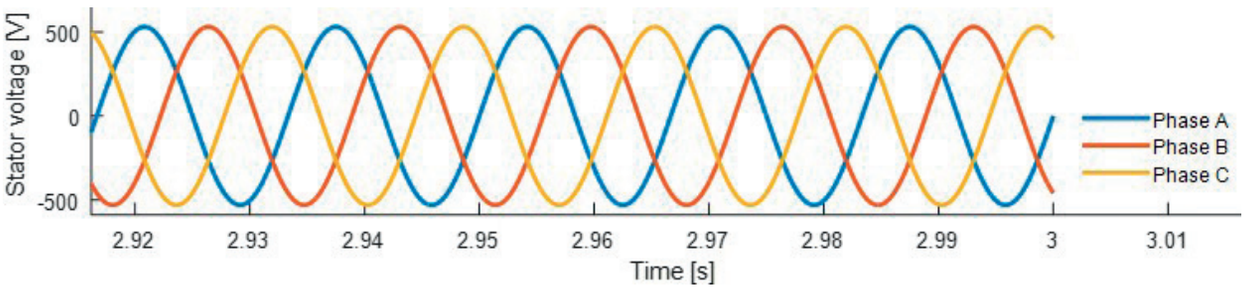

Figure 9. Stator voltage.

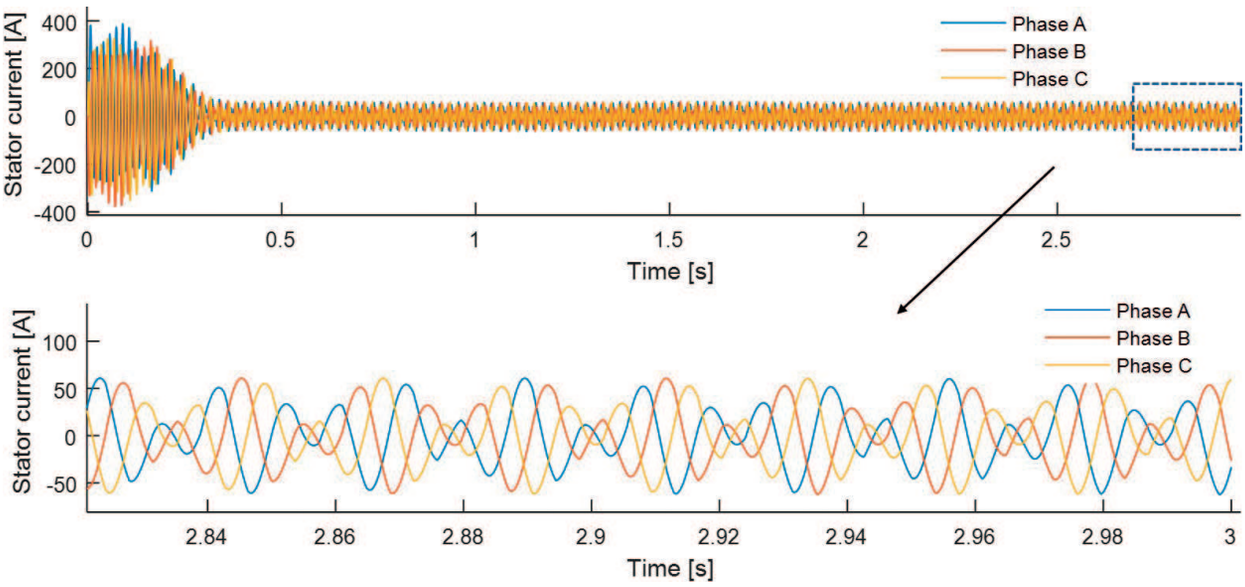

Figure 10. Three-phase stator current in dynamic-state.

http://dx.doi.org/10.5772/intechopen.74584

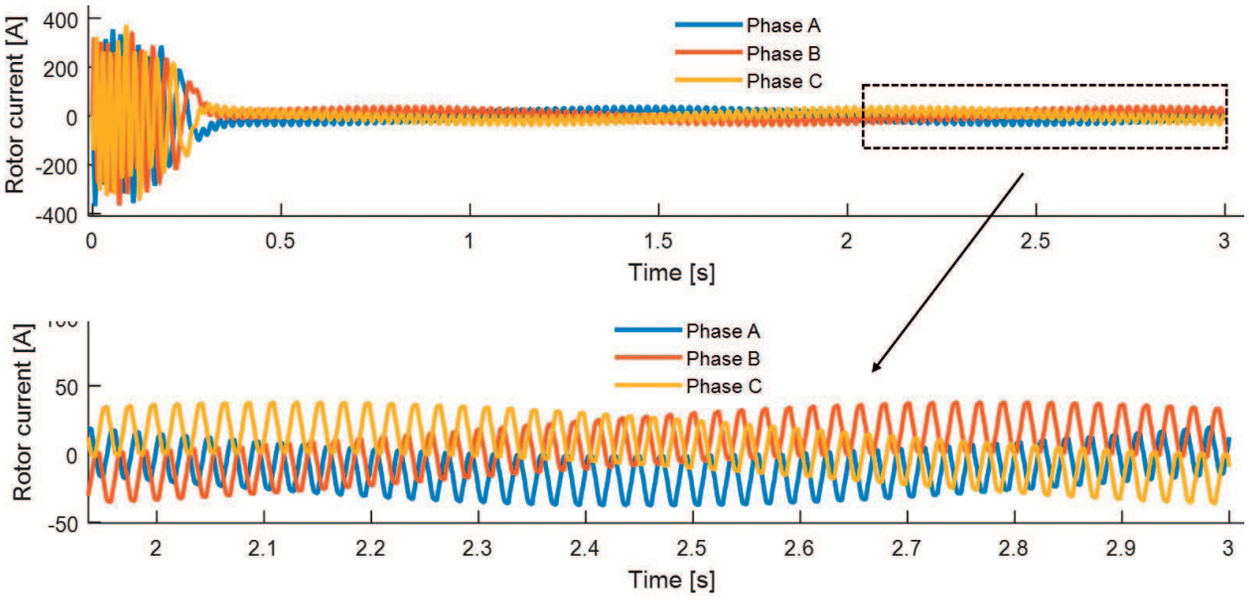

Figure 11. Three-phase rotor current in dynamic-state.

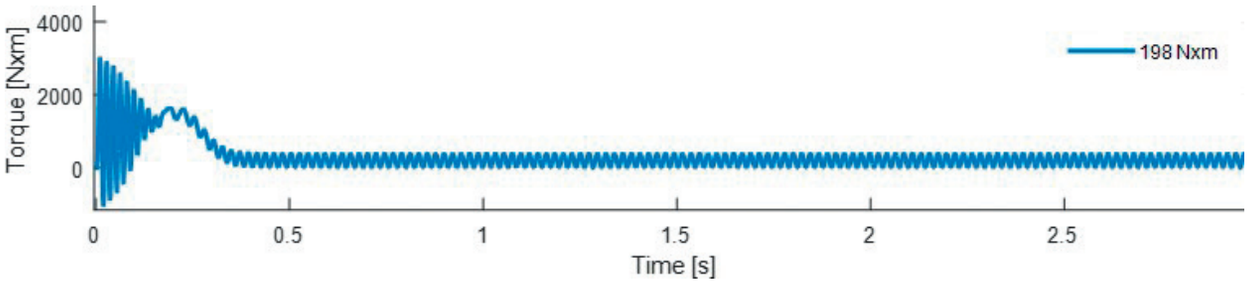

Figure 12. Electromagnetic torque.

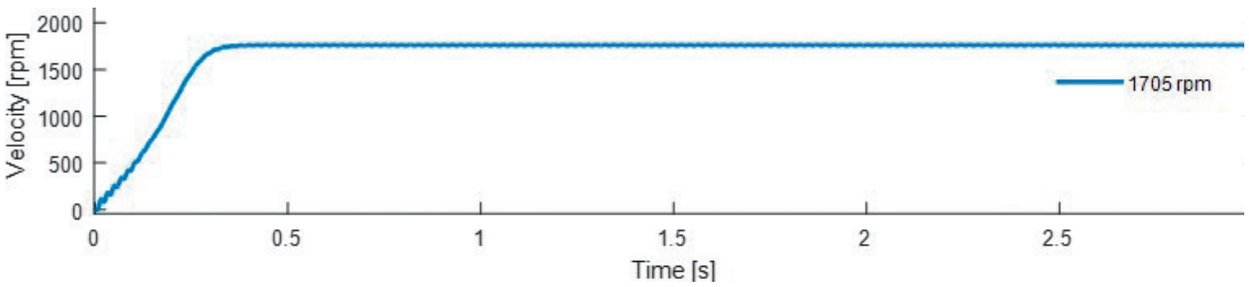

Figure 13. Nominal velocity.

The current waveforms of stator and rotor are obtained from steady-state model and shown in **Figures 14** and **15**, respectively. In addition, an expansion of these currents is made and shown in **Figures 16** and **17**.

Finally, a comparison is made of the forms obtained in both models, both in magnitude and in phase angle, concluding that both models coincide in these aspects. The graphic result of this is shown in **Figures 18** and **19**, respectively.

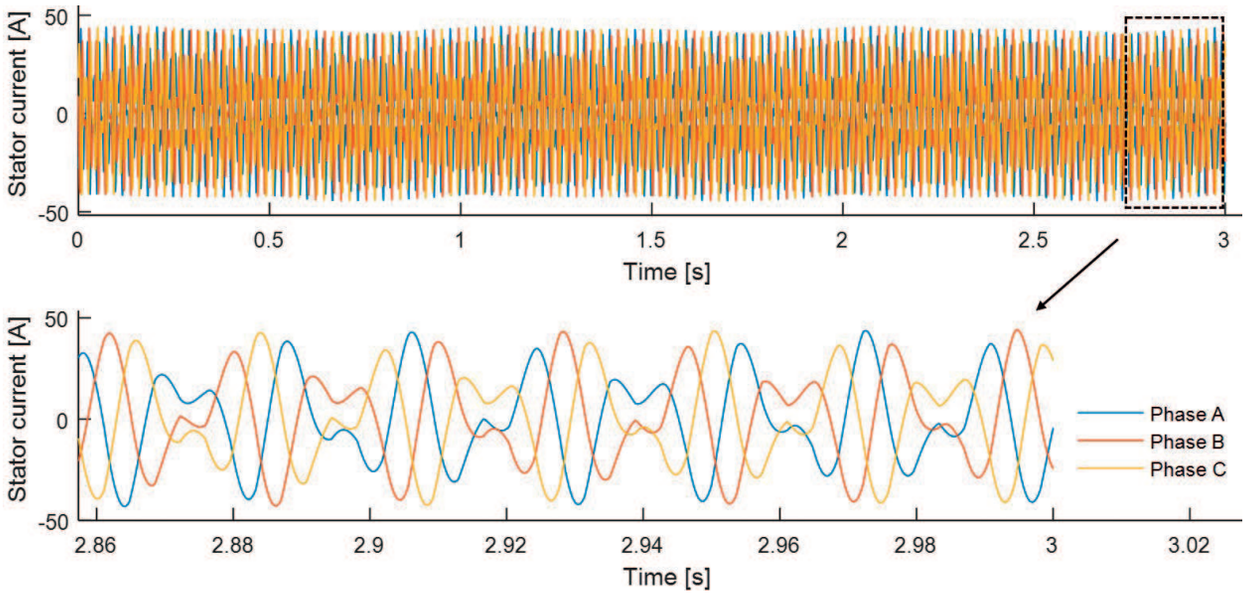

Figure 14. Three-phase stator current in steady-state.

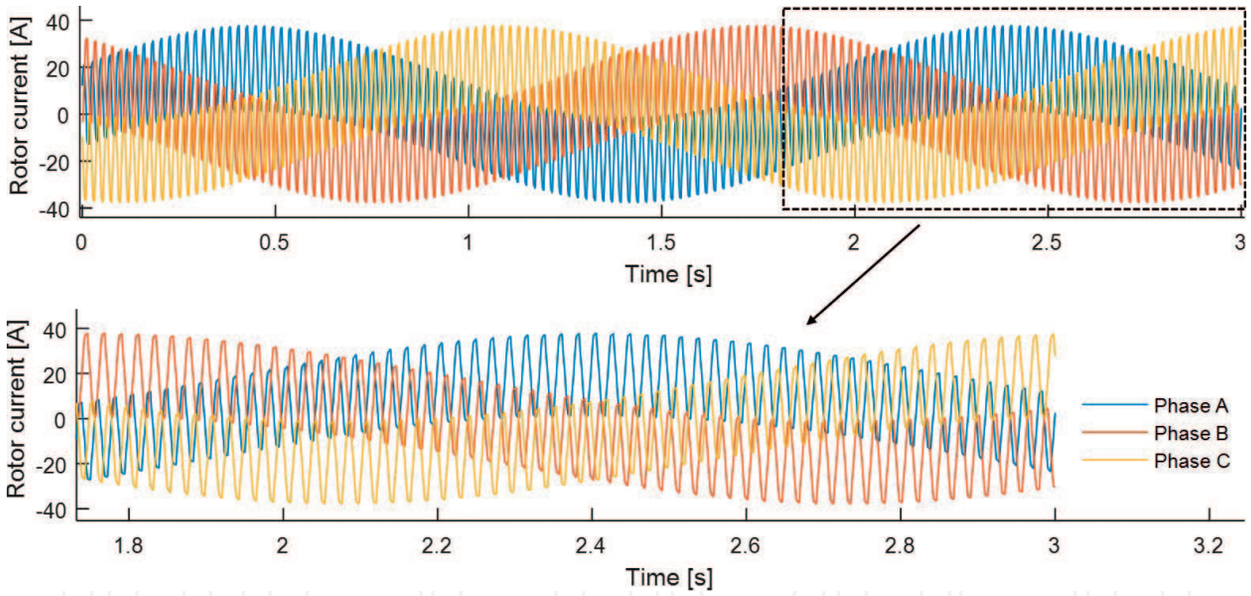

Figure 15. Three-phase rotor current in steady-state.

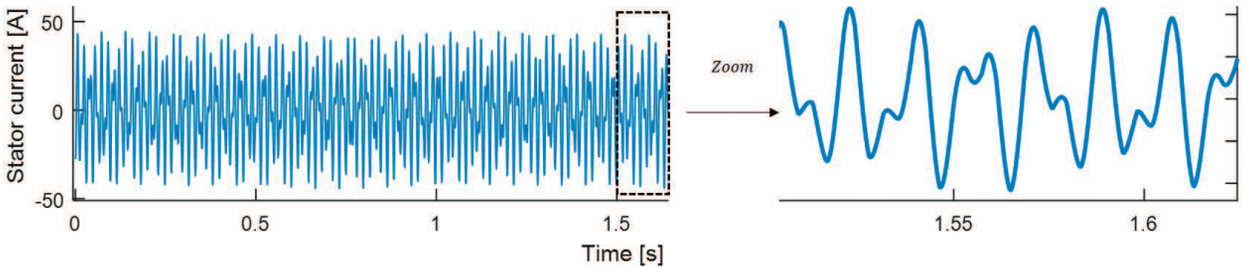

Figure 16. Expansion of the stator current in steady-state.

http://dx.doi.org/10.5772/intechopen.74584

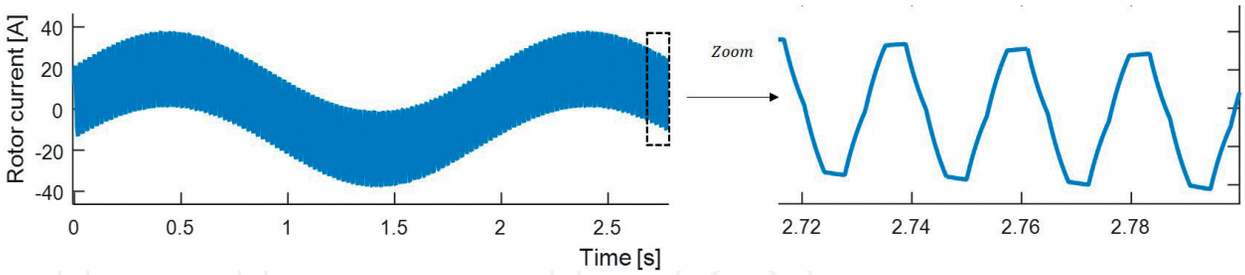

Figure 17. Expansion of the rotor current in steady-state.

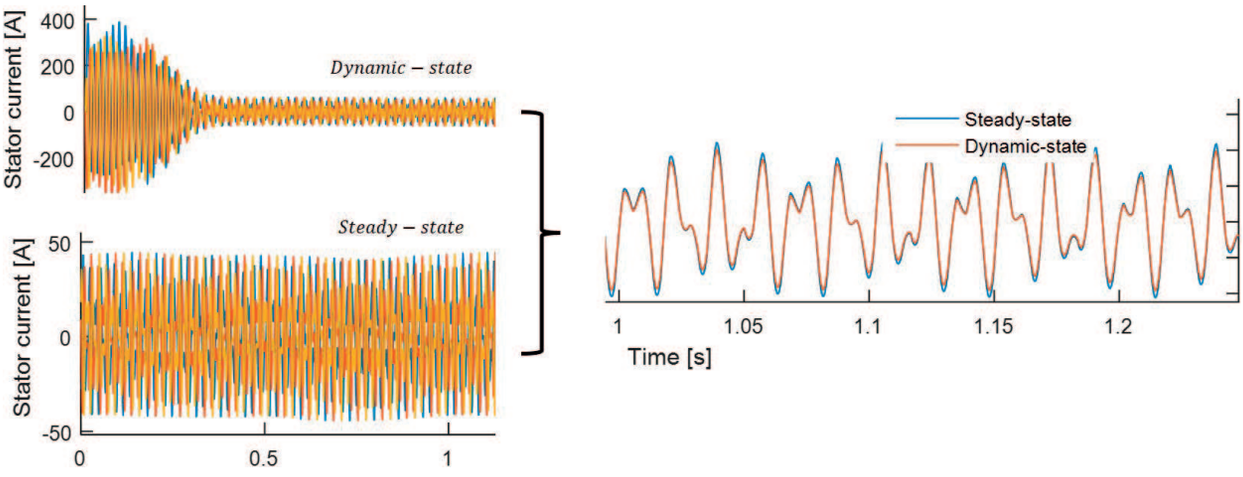

Figure 18. Results comparison of both models: steady-state and dynamic-state, respectively.

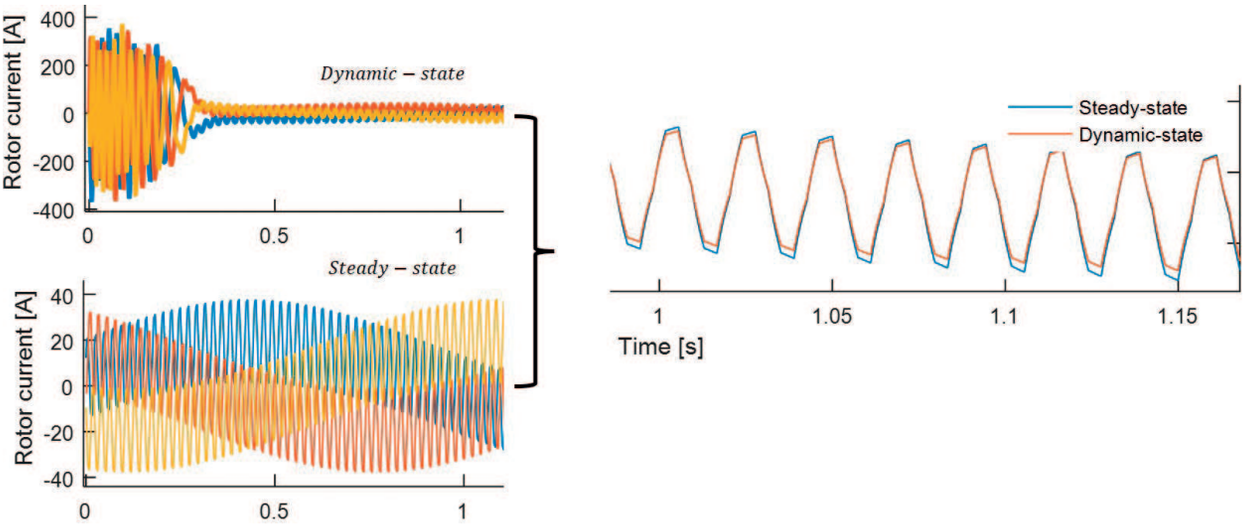

Figure 19. Results comparison of both models: steady-state and dynamic-state, respectively.

5. Incorporation to the electrical network

The integration of wind farms into the network is not an easy problem to solve. Numerous studies have been carried out related to the impact of wind penetration on electric power systems, including those related to stability studies, response of electrical protections and harmonic effects in the electrical network. In some power systems, the penetration of wind energy is rapidly increasing and begins to influence the overall behavior of the system and its stability. In **Figure 20**, it is possible to observe the equivalent diagram of the system to be simulated, which corresponds to the simplification of an induction generator, a frequency converter and typical distribution system. It is presented a three-phase circuit that feeds an industrial load, consisting of a doubly fed induction generator (DFIG), controlled by a back-to-back converter (which injects the harmonic current components).

The presence of harmonics in an electrical power distribution system can bring serious problems, both for the same equipment or system that produces them as for other equipment connected in the same network. The generated harmonic currents interact with the system impedance and cause the voltage distortion, increase the losses and produce effects of overloads connected to the electrical network. Furthermore, they reduce the power factor, given its reactive nature. The presence of harmonic distortion will be more appreciable in some points than in others. However, we can establish that, in general, the effects of harmonics depend on:

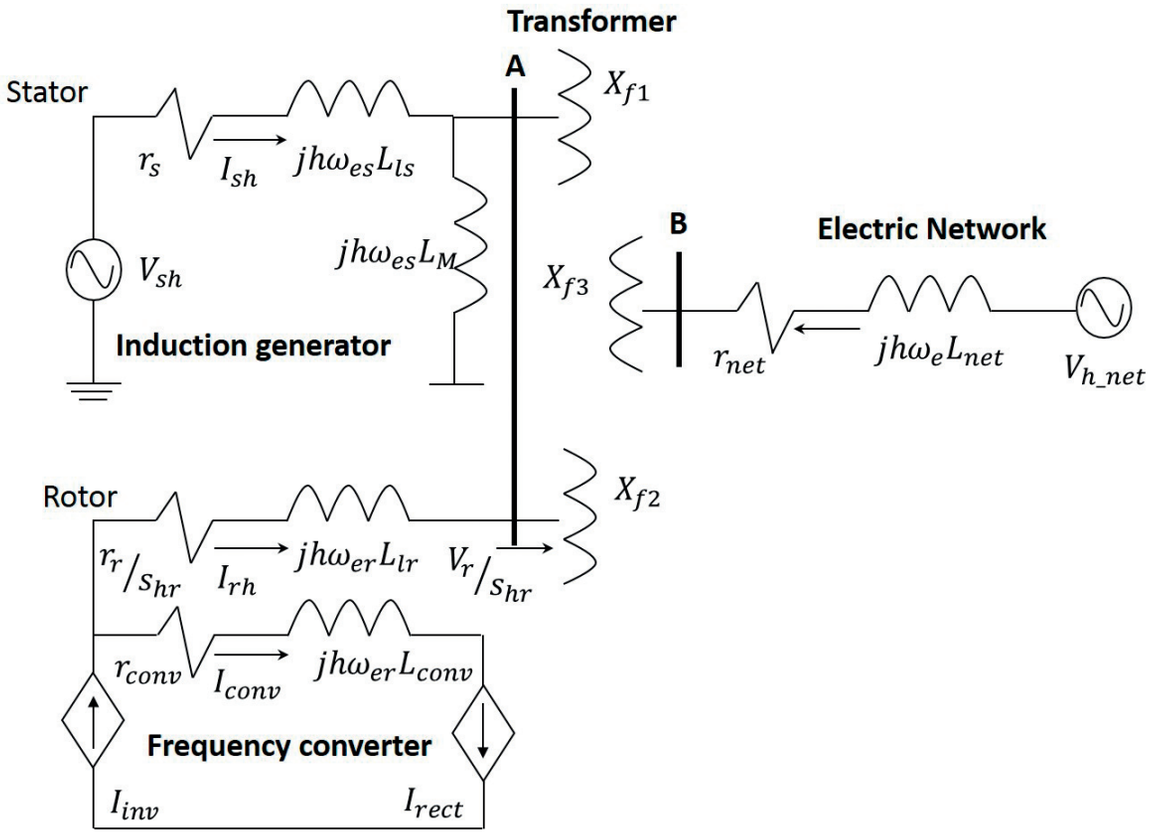

Figure 20. Complete equivalent diagram of WECS connected to the electrical network.

- the elements that generate harmonics, their diversity within the system, the spectral content they inject and their operating regime in time-domain
- the quantity, configuration and values of the elements in the electrical network, both in the time-domain and frequency-domain;
- the sensitivity of the equipment to the presence of harmonic currents or voltages;
- the degree of interest shown by electricity companies and commercial and industrial companies for the harmonic problems that may arise;
- the establishment of norms to set individual total harmonic distortion limits and their compliance on the part of the sectors involved; and
- the effectiveness of standards over time, depending on the technological cases registered in the manufacture of new equipment.

In the study of the effects of harmonics in the distribution systems, it is important to know the propagation paths of the harmonic currents, whose important effect in the system consists in the distortion of the voltage in the different nodes, transferring the harmonic presence to other subsystems. The presence of harmonic voltages results in currents with those harmonic frequencies, which cause additional losses. The induction generator operating with non-sinusoidal voltages cause additional losses due to harmonics. The harmonic losses that occur are losses in stator copper, losses in the core, mechanical losses and losses in the rotor. The largest losses occur on rotor bars (for squirrel cage generator). In addition, harmonic losses are independent of the generator load, but may be much greater than losses due to a pure sine wave, depending on the harmonic content of the applied voltage waveform. These factors raise the temperature of all generator components reducing the efficiency and the useful life. This elevation in temperature may result in excessive heating and may not meet the demands of the load coupled to its axis, or resulting in the destruction of the generator. Harmonic currents cause increased losses in copper for to the skin effect due to their high frequencies, cause insulation stresses, Eddy current losses in the conductive parts and possible resonance at a harmonic frequency between the inductive reactance of the transformer and the capacitance of the line or capacitors for power factor improvement.

The effect of the losses, then, is an increase in the heating of the transformer, which may be significant. Due to behavior of triple harmonic currents in three-phase systems, the three currents of line are in phase, and when they reach the center of a wye connection, they will return through the neutral or ground. This fact, although the three-phase system is perfectly balanced, can cause the heating of cables and connectors when its ampacity is exceeded.

5.1. Power-quality problems of WECS connected to the electrical network

The term 'power quality' refers to voltage and frequency stability, and the absence of various forms of electrical noise (e.g., flicker or harmonic distortion) in the electrical network. Generally, electric companies (and their customers) prefer an AC with a sinusoidal waveform, free of interruptions or disturbances. The consequences of large-scale supply incidents are well

documented. A recent study in the United States has shown that digital industrial and commercial firms are losing $ 45.7 billion per year because of power network disruptions. In all commercial sectors, it is estimated that between 104,000 and 164,000 million dollars are lost due to interruptions and another 15,000–24,000 million dollars because of other power quality problems in the network. Many problems in the supply originate in the electric network that with its thousands of miles of transmission is subject to climatic conditions such as hurricanes, storms with snow, ice and floods, along with equipment failures, traffic accidents and major operations of connection.

The power quality study and ways to control it is a topic of interest for electricity suppliers, large industrial companies, businesses and even residential users. The study has intensified as teams have become increasingly sensitive to even minimal changes in voltage, current and frequency in the supply. The Institute of Electrical and Electronics Engineers (IEEE) has developed a standard that includes definitions of energy disturbances. The standard (Standard 1159–1995 of the IEEE, IEEE Recommended Practice for Monitoring Electric Power Quality) describes many problems of the power quality. Regarding the wind sector, there are regulations that regulate the limits for this type of problems, as indicated by the IEC 61400-21 standard. The IEC–61400-21 standard provides recommendations for preparing the measurements and assessment of power-quality characteristics of wind turbines. The measurement procedures described in the IEC61400-21 standard are valid to test the power-quality characteristic parameters for the full operational range of a wind turbine, connected to a MV or HV network with fixed frequency within ±1 Hz, sufficient active and reactive power regulation capabilities and sufficient load to absorb the wind power production.

5.1.1. Start and stop of the wind turbine

Most of the electronic wind turbine power controllers are programmed so that the turbine runs in no-load at low wind speeds (if it were connected to the network at low wind speeds, in fact it would work as an engine). Once the wind becomes strong enough to rotate the rotor and generator at its rated speed, it is important that the turbine generator be connected to the power network at the appropriate time. If this is not the case, only the mechanical strength of the multiplier and the generator will be present to prevent the rotor from accelerating, and eventually it will be packed (there are various safety devices, including fail-safe brakes, in the case that the of correct start fail).

5.1.2. Soft-started with thyristors

If a high-power wind turbine is connected to the electrical network by means of a normal switch, a partial dimming would be observed (due to the current required to magnetize the generator), followed by a power peak, due to the generator current overloading. Another unpleasant side effect when using 'hard' switches would be to apply extra wear to the multiplier, since the generator connection would act as if the mechanical brake of the turbine were suddenly activated. To avoid this situation, modern wind turbines have a soft-start; they are connected and disconnected from the electrical network gradually by means of thyristors, a type of semiconductor continuous switch that can be controlled electronically. Thyristors lose

about 1–2% of the energy that passes through them. Thus, modern wind turbines are usually equipped with a switch called 'drift', that is, a mechanical switch that is activated after the turbine has made the soft start. In this way, the amount of energy lost is minimized.

5.1.3. Weak electrical network

If a turbine is connected to a weak electrical network (i.e., it is very far in a remote corner of an electrical network with a low-power transport capacity), there may be some problems of partial obscuration and/or power overvoltage. In these cases, it may be necessary to reinforce the electrical network to transport the AC from the wind turbine. The local power company is experienced in dealing with these voltage problems, as they are the exact reflection of what happens when a large user (e.g., a factory with large electric motors) is connected to the electrical network.

5.1.4. Islanding

'Islanding' is a situation that can occur if a section of the electrical network is disconnected from the main electrical network, as would happen by accidental or intentional tripping of a large circuit breaker in the network (e.g., due to stoppages in the network electrical supply or short-circuits in the network). If the wind turbines continue to operate in the part of the network that has been isolated, it is very likely that the two separate networks are not in phase after a short interval of time. The restoration of the connection to the main power network can cause huge overcurrent's in the wind turbine network and generator. This would also cause a great release of energy in the mechanical transmission (i.e., in the axes, the multiplier and the rotor), as would a 'hard connection' from the generator of the turbine to the electrical network. Thus, the electronic controller will have to constantly monitor the voltage and frequency of the AC of the network. In the event that the voltage or frequency of the local network are within certain limits for a fraction of a second, the turbine will automatically disconnect from the network, and immediately afterwards it will stop (normally activating the aerodynamic brakes).

The distributed generation (generation of electricity through of solar panels, wind farms, etc.), is increasingly having a greater presence in the world, in the case of the sector of self-consumption and injection of surplus energy into the network. This factor causes that the energy systems supplier has more advanced control means to verify the variations of loads that cause important fluctuations in the parameters of the voltage, injection of harmonics, change in the power factor, greater technical losses, among others. Therefore, it is advisable to make a power-quality study in an industry, commerce or home. This analysis must be done with high-resolution RMS equipment in order to detect and accurately measure the different parameters mentioned.

5.2. Case study 2. DFIG excited with three-phase *back-to-back* converter SPWM to improve the power quality

For this case, the generator is excited in the stator windings with a sinusoidal three-phase balanced voltage source of 460 V at 60 Hz shown in **Figure 9** and rotor winding is excited with a quasi-sine voltage source of 50 V at 45 Hz to which the SPWM switching technique was

applied. The stator and rotor current waveforms obtained from dynamic-state are shown in **Figures 21** and **22**, respectively. An expansion of these currents is made once they have reached their steady-state.

The current waveforms of stator and rotor are obtained from steady-state model and shown in **Figures 23** and **24**, respectively. In addition, an expansion of these currents is made and shown in **Figures 25** and **26**.

Finally, a comparison is made of the forms obtained in both models, both in magnitude and in phase angle, concluding that both models coincide in these aspects. The graphic result of this is shown in **Figures 27** and **28**, respectively.

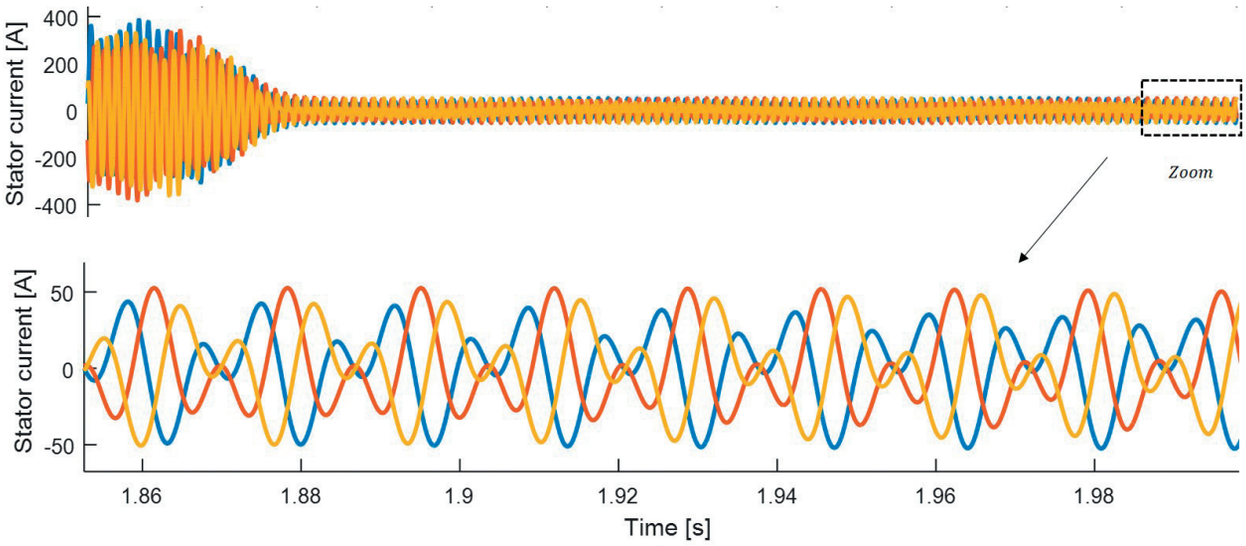

Figure 21. Three-phase stator current in dynamic-state.

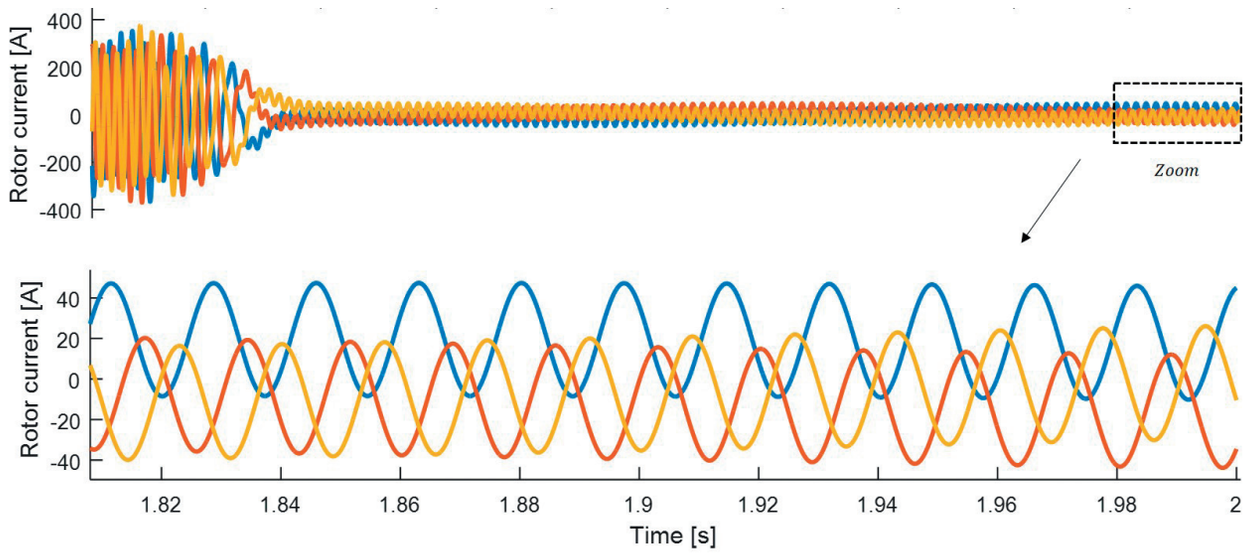

Figure 22. Three-phase rotor current in dynamic-state.

http://dx.doi.org/10.5772/intechopen.74584

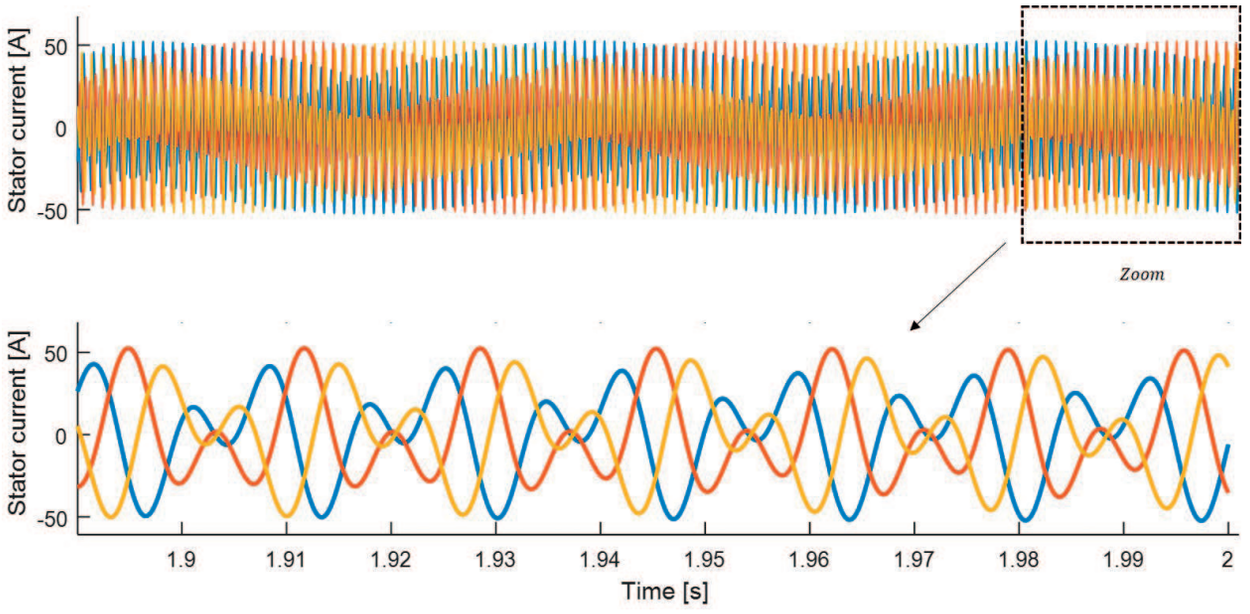

Figure 23. Three-phase stator current in steady state.

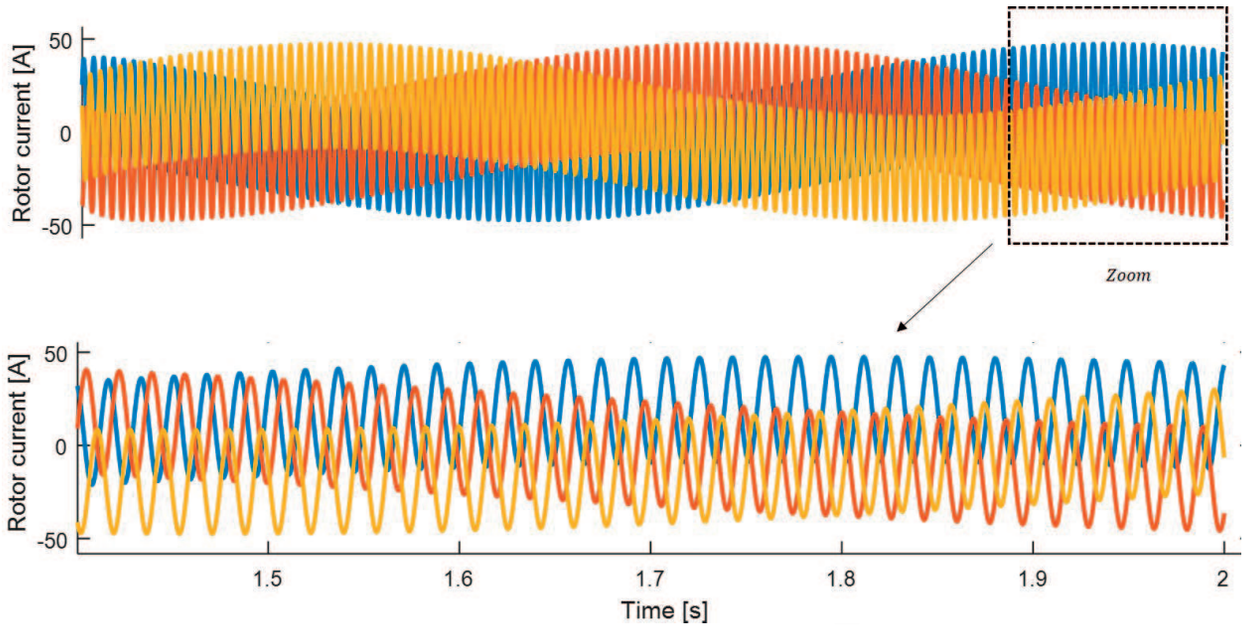

Figure 24. Three-phase rotor current in steady state.

5.3. Analysis of simulation results

The doubly fed induction generator (DFIG) interconnected to the electric network is simulated based on a steady-state model. This proposed model consists of the integration of induction generator, frequency converter and the electric network. Each of those sections is then analysed.

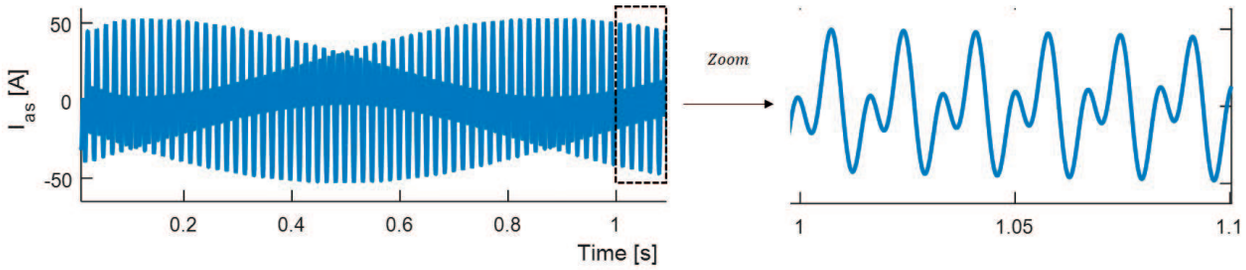

Figure 25. Zoom of **Figure 23**.

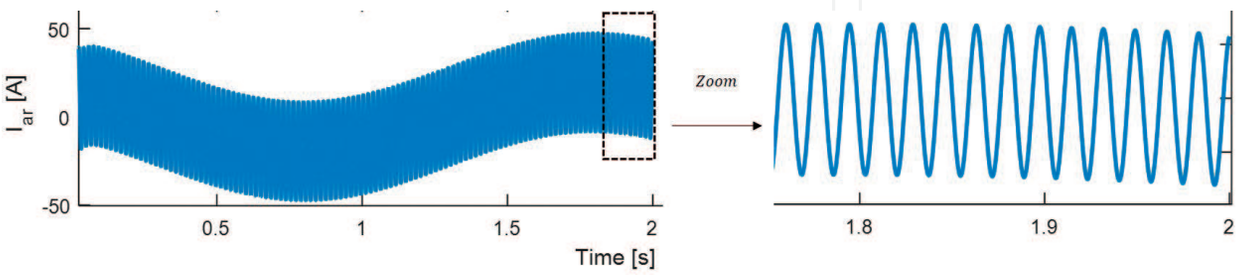

Figure 26. Zoom of **Figure 25**.

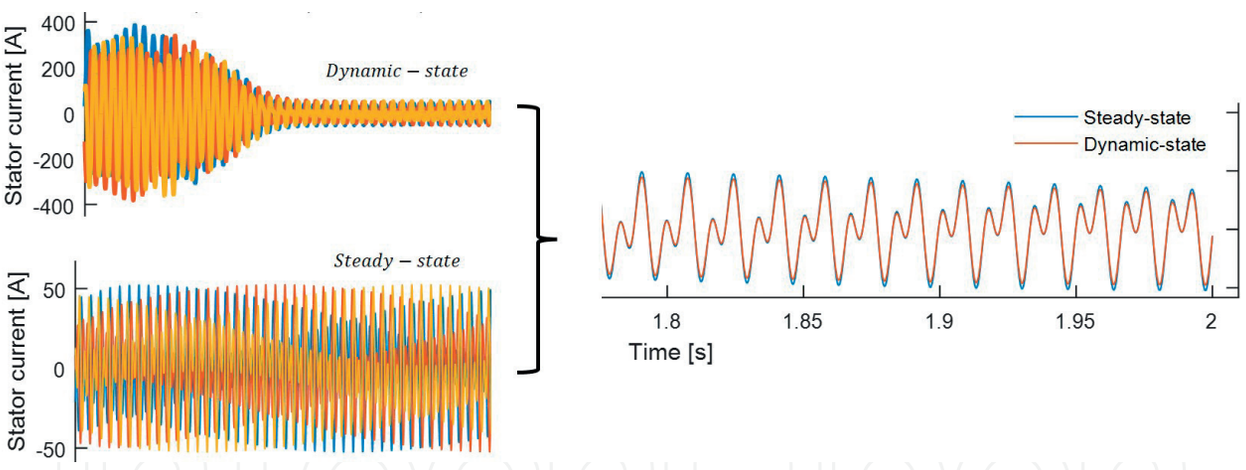

Figure 27. Results comparison of both models: steady-state and dynamic state, respectively.

5.3.1. Rotor-side non-sinusoidal voltage source

Once the harmonic slip for each harmonic signal is determined, the frequencies generated in the rotor-side non-sinusoidal voltage source are obtained as shown in **Table 2**. **Figure 29** shows the frequency spectrum of rotor side non-sinusoidal voltage source. There are harmonics of the order $(6h \pm 1)$ where the signs + and **–** express the positive and negative sequences $(-5, 7, -11\ldots)$; these components generate rotating magnetic fields with the identical or opposite direction of the fundamental field. The rotor voltage during commutation is equal to half of the sum of two-phase voltages that are under commutation with the rotor-line voltage being zero in this period.

http://dx.doi.org/10.5772/intechopen.74584

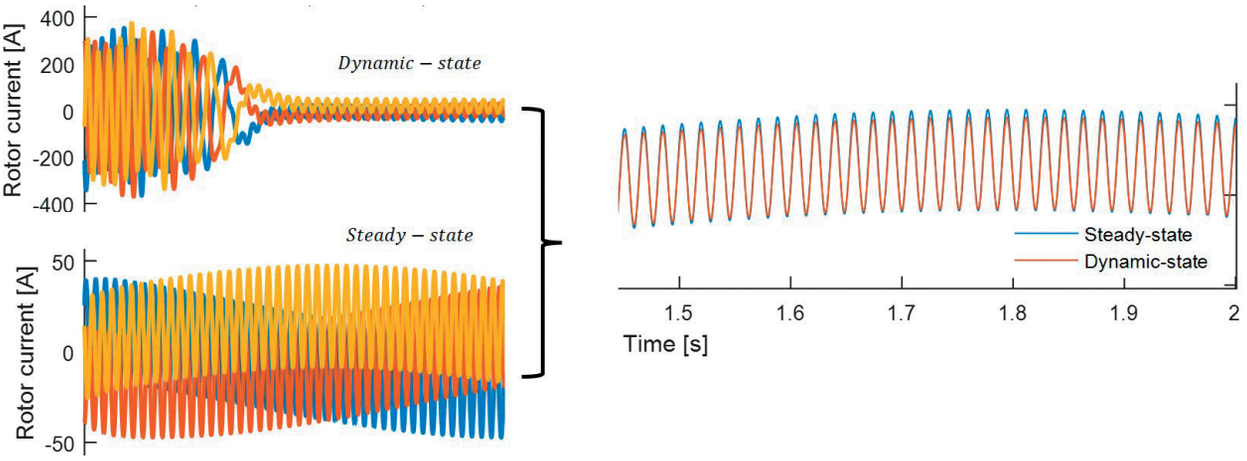

Figure 28. Results comparison of both models: steady-state and dynamic state, respectively.

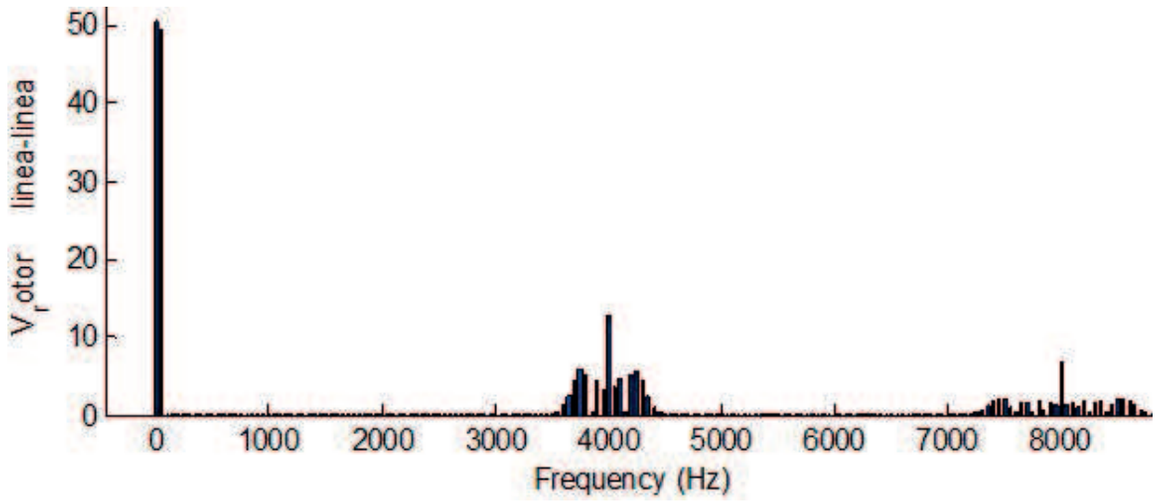

Figure 29. Frequency spectrum of rotor side non-sinusoidal voltage source.

$$f_{hr} = |1 \pm 6h|s_{hr}f_f = |1 - 6(5)| \times 1.21 \times 8.24 = 289.14\ Hz$$

$$f_{hr} = |1 \pm 6h|s_{hr}f_f = |1 + 6(7)| \times 0.96 \times 8.24 = 340.14\ Hz$$

$$f_{hr} = |1 \pm 6h|s_{hr}f_f = |1 - 6(11)| \times 1.32 \times 8.24 = 706.992\ Hz$$

$$f_{hr} = |1 \pm 6h|s_{hr}f_f = |1 + 6(13)| \times 0.97 \times 8.24 = 631.43\ Hz$$

$$f_{hr} = |1 \pm 6h|s_{hr}f_f = |1 + 6(76)| \times 0.9811 \times 8.24 = 3683.29\ Hz$$

$$f_{hr} = |1 \pm 6h|s_{hr}f_f = |1 - 6(80)| \times 1.0198 \times 8.24 = 4022.34\ Hz$$

$$f_{hr} = |1 \pm 6h|s_{hr}f_f = |1 + 6(158)| \times 0.993 \times 8.24 = 7787.390\ Hz$$

$$f_{hr} = |1 \pm 6h|s_{hr}f_f = |1 - 6(159)| \times 1.0173 \times 8.24 = 8002.05\ Hz$$

5.3.2. Electrical network analysis

The network voltage could only be influenced by non-ideal voltage modulation, if the power of the modulated source is in the same class as the network. However, the harmonic current flow over the network generating always-harmonic voltage, which shows undesired effects in the network, independent from the power of the harmonic current source. This means, that harmonic currents are always of high interest for the resulting power quality of the electrical network. For this case, a harmonic voltage and harmonic current of the network is considered. **Figures 30** and **31** present the network current and the network voltage, respectively.

5.3.3. Stator and rotor current analysis

The stator current waveform is shown in **Figure 23** where it is observed that it contains considerable harmonic components. The interaction between the rotor flux harmonics and the fundamental flux in the air-gap induces currents in the stator which are not integer multiple of the supply frequency. These are commonly called inter-harmonic with stator current fluctuation. The harmonic in the rotor are induced in the stator due to the dominant rotor harmonics (harmonic numbers are fifth and seventh).

The behavior of the rotor current in steady-state is shown in **Figure 25**. The ripples on the rotor current and its large rate of variation result in pulsed voltage waveforms. The rotor harmonic current establishes rotating magnetic fields in the air-gap, inducing currents of corresponding frequencies to the stator winding. It is known that the 6 h + 1 harmonics of the rotor current set

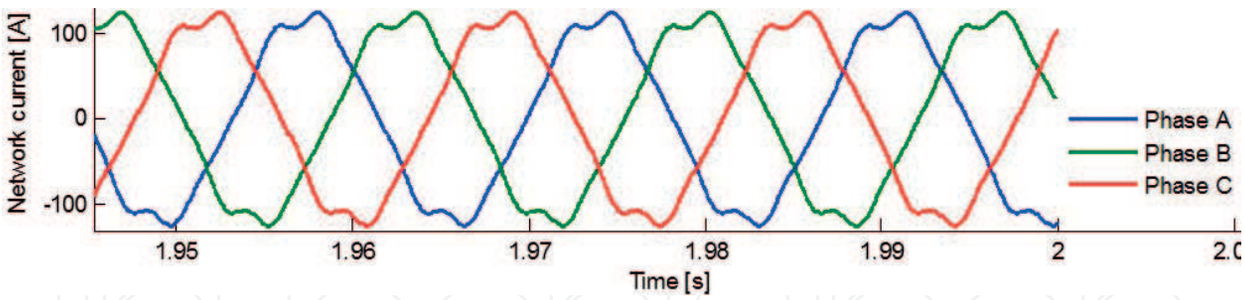

Figure 30. Electrical network current.

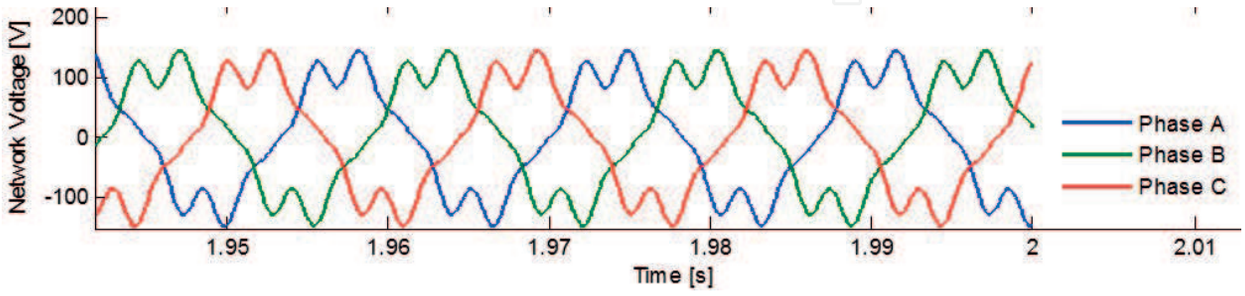

Figure 31. Electrical network voltage.

up positive sequence magnetomotive force (MMF) waves, rotating in the same direction as the fundamental rotor MMF, whereas the $6h-1$ harmonics establish negative sequence MMFs. Since the fundamental rotor MMF rotates in the same direction as the rotor for s > 0 (motoring mode) and in the opposite for $s < 0$ (regenerative mode), the angular velocity of the rotating MMFs relative to the rotor is always $(1 \pm 6h)sf_{es}$. Adding the rotor velocity, $(1 - s)f_{es}$, yields the velocity of the rotating MMF waves relative to the stator and, therefore, the frequency of the induced harmonic currents is obtained with: $f_{es\_h} = |1 \pm 6hs|f_{es}$, $h = 0,1,2,3\ldots$. Similarly, the rotor side-band frequencies due to the rotor-side converter harmonics also set up MMF waves, rotating at $[(1 \pm 6h)s \pm 6m]\, f_{es}$, with respect to the rotor. The frequency of the induced harmonic currents to the stator is then: $|1 \pm 6hs \pm 6_m|f_{es}$, h, $m = 0,1,2,3\ldots$. Since the slip s is non-integer, the harmonic content of stator current consists mainly of sub- and inter-harmonics, which create undesirable effects on the supply system. For instance, low-frequency sub-harmonics appear as unidirectional components superimposed on the phase currents, while sub- and inter-harmonics neighbouring to the supply frequency may create a beat effect on the stator current magnitude. The rotor harmonic current due to the switching of the transistor appear at frequencies $f_{er\_h} = (6h \pm 1)|s|f_{es}$, $h = 0,1,2,3\ldots$, that is, at the 5th, 7th, 11th, 13th … of the fundamental rotor frequency $|s|f_{es}$ $h = 0$ for the fundamental.

The DC current distortion introduced by the network-side converter (at the frequencies f_{dc_h}) is also reflected on the rotor currents, however, resulting in the appearance of additional harmonics. More specifically, each rotor-side converter-related harmonic frequency f_{dc_h} of the DC current is superposed on the harmonics f_{er_h} of the rotor current, resulting in the appearance of two 'side-bands' at frequencies $|f_{er\_h} \pm f_{dc\_h}|$. Hence, the full harmonic content of the rotor current is given by: $f_{es\_h} = |(6h \pm 1)s \pm 6m|f_{es}$, $h,m,$ = 0,1,2,3….

It explains only the harmonic frequencies at 20 Hz (fundamental rotor frequency), 100, 140, 220, 260, 340 and 380 Hz, corresponding to h = 1, 5, 7, 11, 13, 17 and 19. For instance, the spectral lines at 280 and 320 Hz result from the interaction of the 20 Hz fundamental rotor frequency with the basic inverter DC harmonic at 300 Hz $[20 \pm 300]$Hz, for $h = 0$ and $m = 1$]. **Table 4** resumes the harmonic currents in the induction generator for this research. Note that the waveform of current presented in **Figures 23** and **25** has been attained from the current shown in **Table 4**.

5.4. Case study 3. High-power DFIG excited with *back-to-back* converter

Finally, a last case study of the doubly fed induction generator is presented. To validate the proposed model, a three-phase generator of 372.8 kW, 2300 V and 93.8 A at 60 Hz is used. The rotor windings are excited with a quasi-sine voltage source of 500 V at 45 Hz. The induction generator parameters are shown in **Table 4**.

For this case study, a $T_m = 1980\ N$ in the induction generator was used. The stator and rotor current waveforms obtained from dynamic-state are shown in **Figures 32** and **33**, respectively.

The electromagnetic torque and the nominal velocity reached by the generator are shown in the **Figures 34** and **35**, respectively. The current waveforms of stator and rotor are obtained

Case study	Stator current				Rotor current			
	Sequence (+, –, 0)	Magnitude (%)	Angle (°)	Frequency (Hz)	Sequence (+, –, 0)	Magnitude (%)	Angle (Degrees)	Frequency (Hz)
Case I	+	100	−64.3	60	+	100	160.2	19.8
		31.2	176.2	180	–	16	205.1	100
	–	19.7	172.4	300	+	14	197.7	140
	+	14.3	186.4	420	–	12	128.1	220
	+	3.6	52.9	72.6	+	11	201.7	260
	–	2.1	−3.5	151.2	–	2.3	188.7	340
	+	1.1	−6.8	210.7	+	2	192.8	380
	–	0.74	7.2	330.1	–	1.7	195	460
	+	0.56	186.1	408.2	+	1	175	500
	–	0.23	192.1	533.8	–	0.9	178.2	580
	+	0.21	200	596.6	+	0.8	195	620
	–	0.08	202	722.2	–	9.6	209.8	1540
	+	0.07	203.7	750	+	8.2	209.5	1640
	–	0.02	206.2	910.6	–	4.9	236.4	3140
	+	0.01	212.8	973.4	–	4.2	237.9	3160

Table 4. Summary of the harmonic current for the case study.

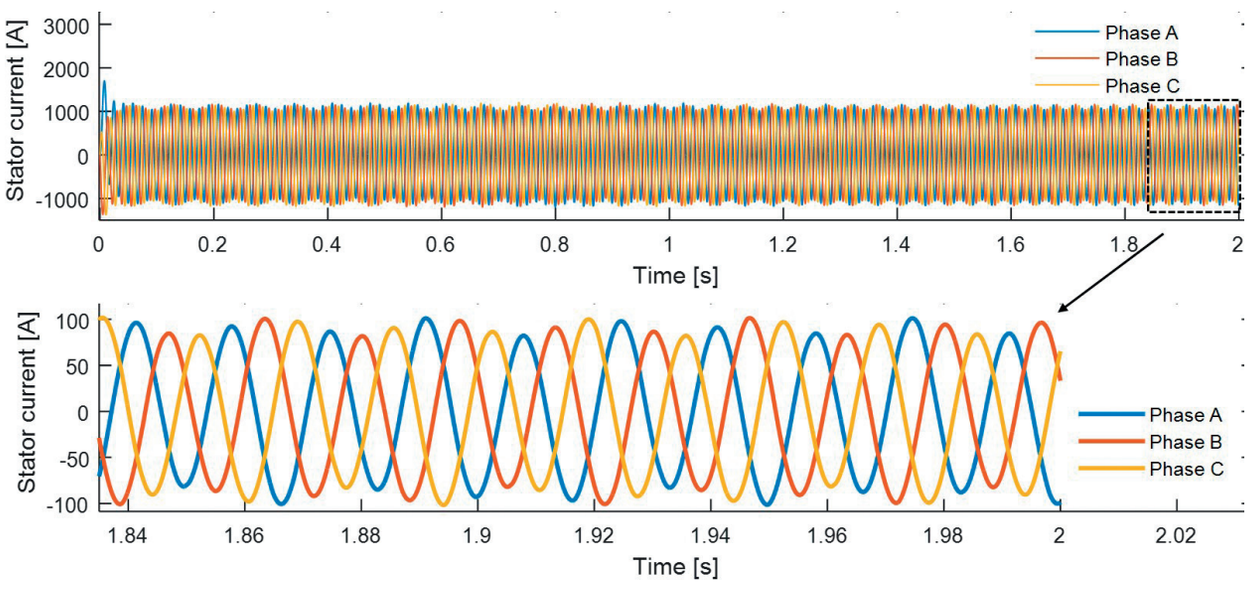

Figure 32. Three-phase stator current in dynamic-state.

http://dx.doi.org/10.5772/intechopen.74584

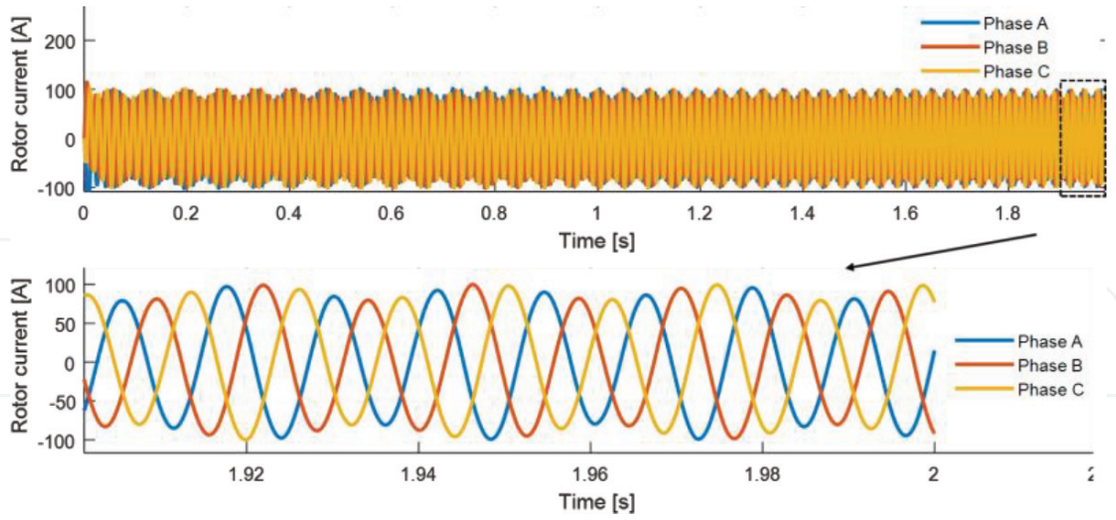

Figure 33. Three-phase rotor current in dynamic-state.

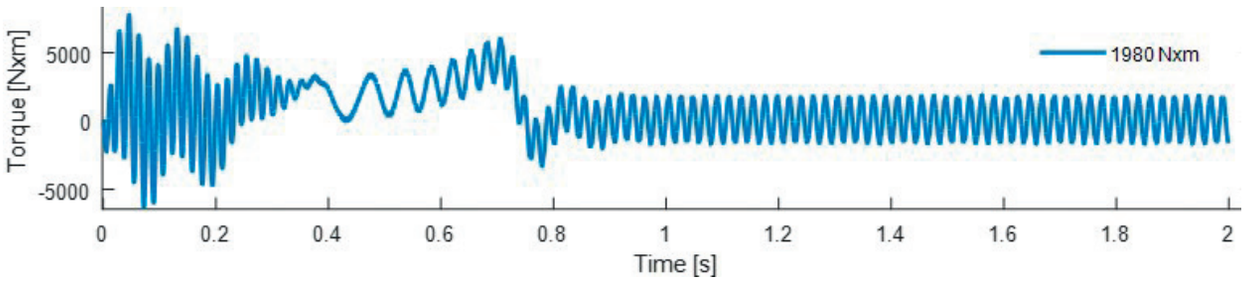

Figure 34. Electromagnetic torque.

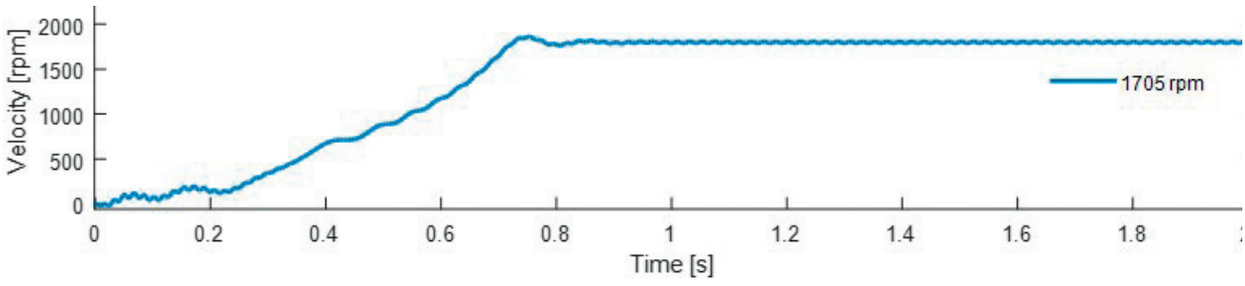

Figure 35. Nominal velocity.

from steady-state model and shown in **Figures 36** and **37**, respectively. Also, an expansion of these currents is made and shown in **Figures 38** and **39**.

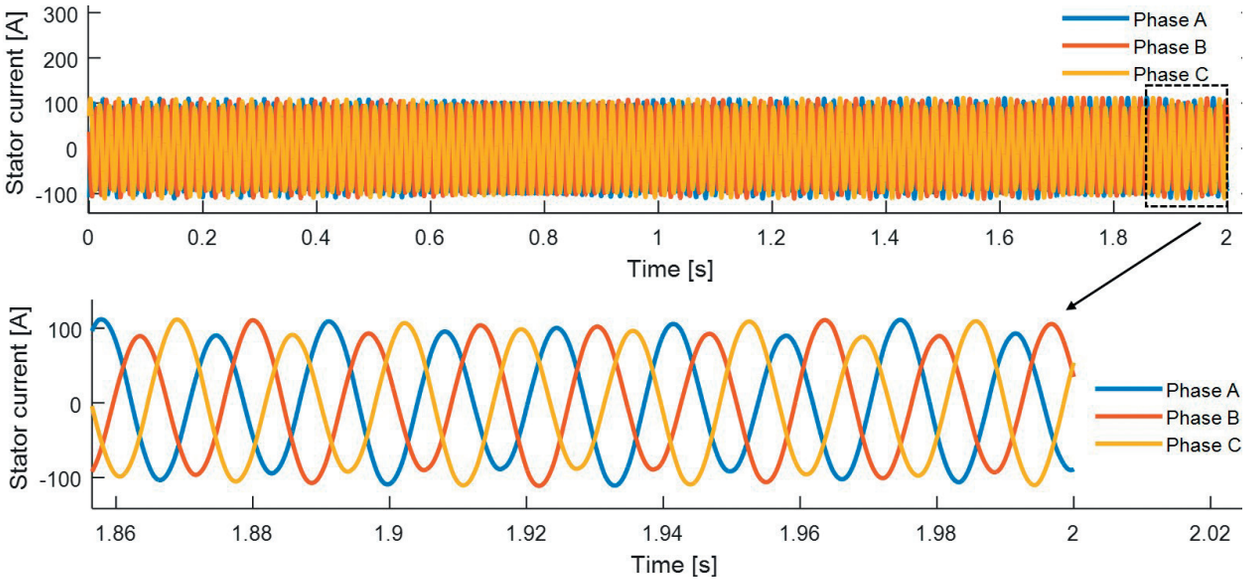

Figure 36. Three-phase stator current in steady-state.

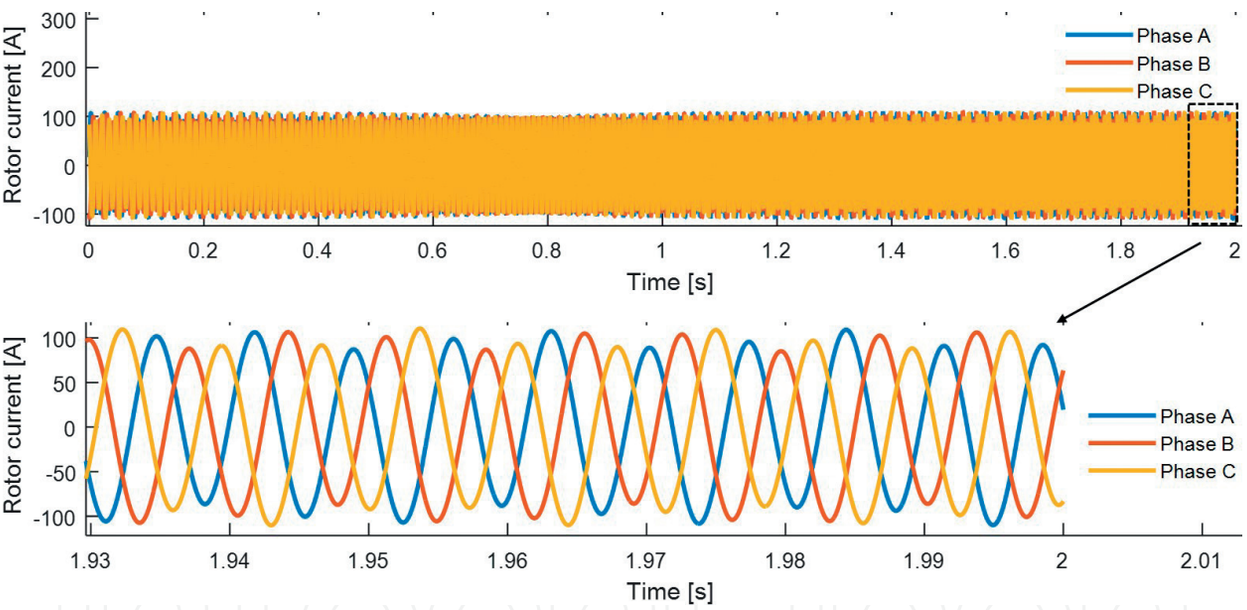

Figure 37. Three-phase rotor current in steady-state.

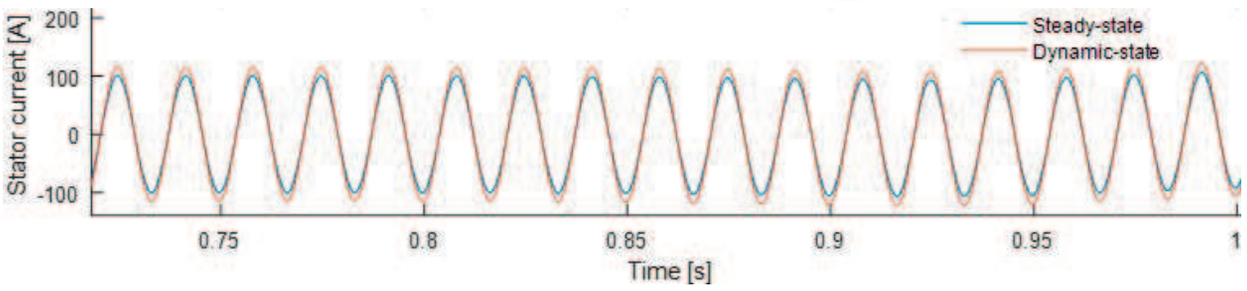

Figure 38. Results comparison of both models: steady-state and dynamic state, respectively.

http://dx.doi.org/10.5772/intechopen.74584

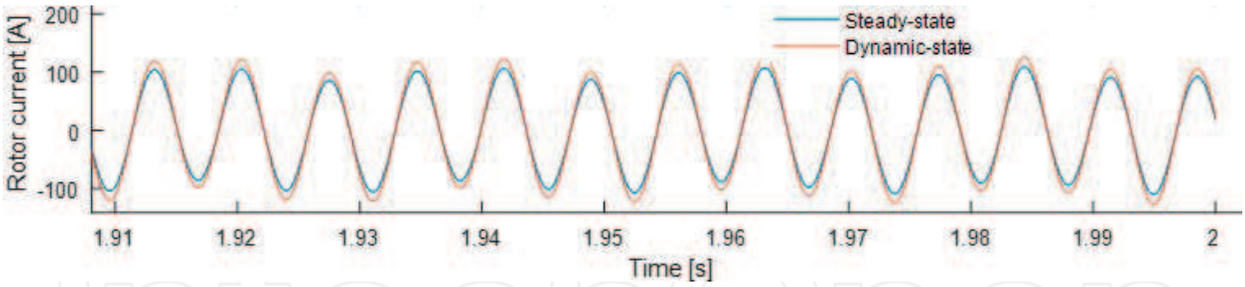

Figure 39. Results comparison of both models: steady-state and dynamic state, respectively.

Parameters	**500 HP/372.8 kW**
Wind speed	10 m/s
Number of poles	4
Rotor speed	1773 rpm
Inertia	11.06 kg·m^2
Nominal line current	93.6 Amps
Nominal line-to-line voltage	2300 Vrms
Nominal torque	1980 N.m
Nominal frequency	60 Hz
Stator resistance, r_s	0.262 Ω
Stator inductance, L_{ls}	0.0032 H
Rotor resistance, r_r	0.187 Ω
Rotor inductance, L_{lr}	0.0032 H
Magnetizing inductance, $L_{mr} = L_{ms}$	0.1432 H

Table 5. Parameters of a 500 HP induction generator.

Noted that the results obtained from the proposed model (steady-state) are compared with those obtained from the simulated complete model (dynamic) ones the steady-state has been reached (**Table 5**).

6. Conclusion

Based on the results of this research, we propose a wind turbine model based on a double-fed induction generator for harmonics propagation studies. This model consists of three stages: analysis of the induction generator, analysis of the frequency converter and analysis of the electric network. It should be mentioned that the models were developed in steady-state and dynamic-state. Finally, the three stages are integrated for the development of a single model for

the harmonic analysis of the double-fed induction generator interconnected to the electrical network. The results indicate harmonic and non-harmonic currents can exist in both generator windings depending on the slip and the fundamental frequency in both voltage sources. The results of the steady-state simulation were compared with the results in dynamic-state model obtaining great similarity in the waveforms of the currents in the stator and rotor, in both magnitude and phase angle resulting in a proper model for harmonic and non-harmonic analysis of the doubly fed induction generator (DFIG) which can be used for 'harmonic' analysis in electrical power systems.

Author details

Emmanuel Hernández Mayoral*, Miguel Ángel Hernández López,
Hugo Jorge Cortina Marrero and Reynaldo Iracheta Cortez

*Address all correspondence to: emanuel.mayoral7@gmail.com

Universidad del Istmo, Av. Universitaria s/n Bo. Santa Cruz Tagolaba, Tehuantepec, Oaxaca, Mexico

References

[1] Arrillaga D, Bradley A, Bodger PS. Power System Harmonics. 2nd ed. California: John Wiley & Sons; 1989. p. 500

[2] Randall RB. Application of B and K Equipment to Frequency Analysis. 1st ed. USA: Bruel and Kjaer; 2003. p. 485

[3] Kreyzig E. Advanced Enginnering Mathematics. 6th ed. USA: John Wiley & Sons; 2010. p. 806

[4] Bergland GD. A Fast Fourier Transform Algorithm for Real Valued Series. Communications of the ACM. 1st ed. England; 1986. p. 710

[5] Carrasco JM, Franquelo LG, Bialasiewicz JT, Member S, Galván E, Guisado RCP, Member S, Ángeles M, Prats M, León JI, Moreno-Alfonso N. Power-electronic systems for the grid integration of renewable energy sources: A survey. IEEE Transactions on Industrial Electronics. 2006;**53**(4):1002-1016

[6] Arcega FJ, Pardina A. Study of harmonics thermal effect in conductors produced by skin effect. IEEE Latin American Transaction. 2014;**26**(1):1488-1495

[7] Hu J, Nian H, Xu H, He Y. Dynamic modeling and improved control of DFIG under distorted grid voltage conditions. IEEE Transaction Energy Conversion. 2011;**26**(1):163-175

[8] Amini J. Novel control method of grid connected converter of doubly fed induction generator to achieve disturbances rejection. In: International Conference on Environment and Electrical Engineering. Washington, DC; 2011. pp. 1-5

[9] Mora-Barajas M, Bañuelos-Sánchez P. Contaminación armónica producida por cargas no lineales de baja potencia: modelo matemático y casos prácticos [dissertation]. Madrid: 2010. p. 111

[10] Comech MP. Análisis y Ensayo de Sistemas Eólicos ante Huecos de Tensión [thesis]. Zaragoza: Universidad de Zaragoza; 2007. p. 100

[11] Boldea. Synchronous Generators. 1st ed. USA: Taylor & Francis Group; 2006. p. 256

[12] Cuevas M. Control Vectorial de un Motor de Inducción Doble Alimentado [thesis]. Mexico: CENIDET; 2003. p. 113

[13] Gamarra. Control de un Generador Doblemente Alimentado para Turbinas Eólicas [thesis]. Universidad Politécnica de Cataluña: Ingeniería Técnica Industrial; 2009. p. 110

[14] Sierra E. Análisis del diseño y control de un generador trifásico doblemente alimentado [thesis]. Chile: Ingeniería Civil Electricista; 2012. p. 152

[15] Hernandez E, Madrigal M. A step forward in the modelling of the doubly fed induction machine for harmonic analysis. IEEE Transaction Energy Conversion. 2014;**29**(3):149-157

IntechOpen